Universidad Politécnica de Cartagena

industriales
etsii UPCT

Method of measuring the water jet diameter

Método de medida del chorro de agua

Titulación: Ingeniería Industrial
Alumno: Jesús Gil Cano
Director: Lorenzo Ros McDonnell

Cartagena, 12 de Septiembre de 2013

Acknowledgements

At the beginning of this master thesis, I would like to thank those people who have made it possible to complete my study.

My parents deserve the greatest thanks. They have given me the opportunity to study and supported me during this.

During my two years here, in Slovenia, many people have helped me. Therefore it seems appropriate at this moment to thank them.

First of all, I would like to thank my mentor prof. Miha Junkar for giving me the opportunity to develop my thesis and for trusting in me from the beginning, the co-mentor Andrej Lebar and the assistant engineer Marko Jerman for supporting me during the work, and to all the personnel of the Laboratory of alternative technologies (LAT) for making me feel as at home.

I would also like to thank the University of Ljubljana for the hospitality during this Erasmus exchange.

I would like to thank my friend Doriana, who helped me with her support that made easier the realization of the paper.

Further, I would like to thank the people who have made the Erasmus life unforgettable, since the two years I spent in Ljubljana have been a great experience.

UDC 621.9:622.232.5:53.08(043.2)

No.: MAG II / 8 E

METHOD OF MEASURING THE WATER JET DIAMETER

JESÚS GIL CANO

Key words: Water Jet (WJ)
Ice Jet (IJ)
Jet Diameter
Imaging processing
Macro photography

Abstract:

Abrasive Water Jet (AWJ) machining is one of the manufacturing technologies with highest market growth. It is a process in which material is removed from a work piece using mineral abrasive particles. Due to this principle, AWJ machining technology produces significant amount of waste products that consists mainly on the mineral abrasive. It is possible to cut softer materials with pure water jet (WJ), but efficiency is then reduced. In order to increase the efficiency of the WJ machining and to make the process more sustainable than AWJ, the Ice Jet (IJ) technology was developed.

The IJ technology aims to supplement the currently used AWJ technology in several applications. Unfortunately addition of liquid nitrogen to a high-speed water jet can cause dispersion of the jet and consequently reduction of cutting efficiency.

Previous experiments in the field of jet diameter measurement have been done by different research groups. In this thesis these methods and the results from the studies based on them, were described and analyzed. This state of the art analysis gave us the knowledge to begin the research on our new method. It also showed that due to possible implementation in industry applications, a quick, easy and affordable technique would be useful. For this reason the phenomenological analysis method to measure the diameter of the water jet was explored.

The new method combines digital image acquisition and processing with digital manipulation of the photography. The main advantages of such method are that the equipment can be cheap and as the method is contactless, it doesn't get destroyed over time. The analysis of the jet can be automatized and the time of the analysis is short. This means that the method could be applied in the production line to measure the wear of the nozzles during the production cycle without causing any delays. This would increase the lifetime of the nozzles, decreasing the production costs and through online modification of the process parameters also its quality.

During the experiments several process parameters such as water pressure, water temperature and diameter of the water nozzle were modified. In order to verify of the new measurement method, the results were compared with results from another method that has already been established before. Therefore the results from gained from this method served as the reference used to evaluate the new method. The reference method measures the jet diameter through the measurement of the jet force.

The experimental setup was built in order to evaluate new measurement method and to compare the novel photographic method with the method which makes use of the load cell to measure the WJ diameter. Setup was built on the machine for ice jet experiments. To illuminate the jet, two high performance light emitting diodes (LED) were used and a consumer digital single lens reflex (DSLR) camera was used to capture the images. In order to make the image acquisition as constant as possible a microcontroller was used to control the LEDs and to trigger the DSLR. Simultaneously a measurement set of WJ force has been made with the load cell. The focus of this work has been on the photographic method. Measurements with load cell were used for validation of the novel method only.

During the experiments two water nozzles were used, five different standoff distances, three different water pressures and three different water temperatures. Regarding photography two different shutter speeds were used throughout all the experiments. Preliminary several combinations of shutter speed and light intensity has been tested in order to obtain optimal experimental conditions.

Evaluation of results was performed in the Matlab software package. More than one thousand images were processed by fitting a custom function to the specific rows of image. Function was Gaussian with additional quadratic, linear and constant term. Function was fitted to five image rows which correspond to five different standoff distances from the water nozzle. At the precisely same distances also radial dependence of WJ force was measured.

It was found, that the method using digital camera and computer evaluation of image can yield good results which are in good correspondence with measurements of WJ diameter obtained by the load cell.

Table of Contents

Table of Figures

Table of tables

Nomenclature

Symbol	Unit	Description
ρ	[kg/m^3]	density
T	[K]	water temperature
α	[1/K]	coefficient of linear expansion
v	[m/s]	speed of water
HB		Brinell hardness
d0	[mm]	water nozzle diameter
λ	[nm]	wavelength
m	[Kg]	mass
L	[m]	lengh
V	[V]	voltage
I	[A]	current
P	[W]	power
CCT	[K]	correlated color temperature
lm	[lm]	typical pulsed Flux
CFM	[dm^3/s]	air flow
v	[dm^3]	volumen
t	[s]	time
EV	[ISO]	exposure value
SS	[s]	shutter speed
σ	[mm]	standard deviation
μ	[mm]	median
h	[m]	height
p	[Pa]	pressure
f		Calibration factor

1 Introduction

Abrasive water jet (AWJ) technology was first commercialized in the late 1980's as a pioneering breakthrough in the area of non-traditional processing technologies. AWJ machining is a rapidly developing technology used in industry for a number of applications, such as cutting, shaping and milling [1].

The main water jetting technologies used by the industry are, WJ and AWJ, which is non-conventional machining processes, where material is removed from a work-piece using a multitude of small abrasive particles [2].

Abrasive water jet (AWJ) is a versatile machining technology in a way that it can be used to machine virtually all materials that we know. One of the drawbacks of the AWJ technology is that it produces a lot of waste product that consists mainly of the mineral abrasive. The latter is being added to the high speed water jet in order to increase its efficiency. These particles also get stuck inside the work piece, thus contaminating it [6]. One of possible solutions is to substitute abrasive particles in AWJ with ice crystals and thus get rid of the majority of material in the waste sludge. Previous experiments from the research done on this field [4], demonstrated the effectiveness of the use of ice particles as a substitute for abrasives.

Another disadvantage of the AWJ technology is that the use of abrasives in the industrial environment is not always possible, because there are kind of applications such as the machining of hygroscopic and chemically reactive materials, as well as when working near high voltage, toxic and radioactive sources; even in process of meat products, the cleaning of sensitive surfaces and biomedical applications [2].

Injection of ice particles into the high speed water jet can be divided into two basic principles which are presented in Figure 1 and 2 [6].

The first principle is by injection of super cooled ice particles which are prepared in advance.

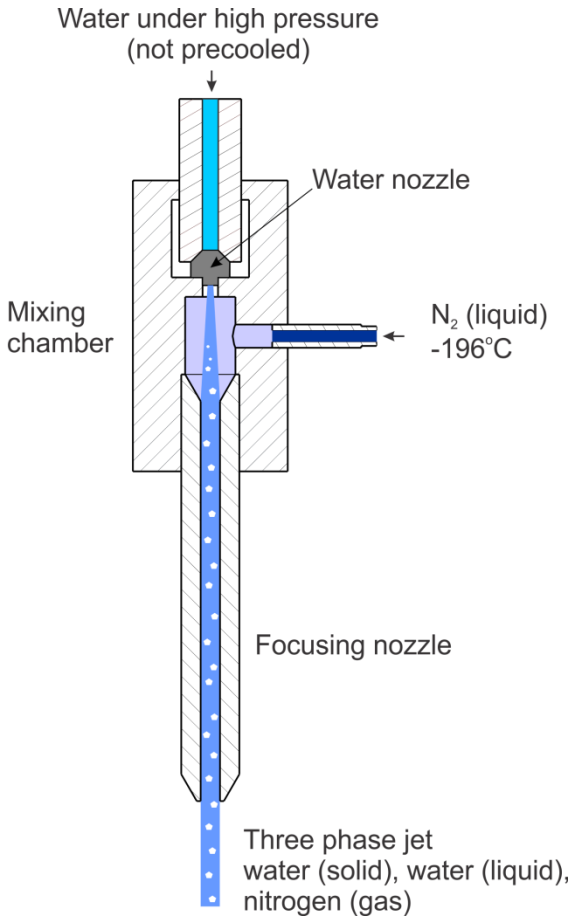

Figure 1: Basic scheme of the Ice Jet cutting head [6].

The second principle is generation of ice particles in-situ, during the cutting process itself by transformation or partial freezing of the water jet. It can be further divided into two methods: the first method is freezing by injection of the liquefied gas (in our case liquid nitrogen) into the mixing chamber and the second method is transformation by sub cooling of the water under high pressure before the water nozzle [6].

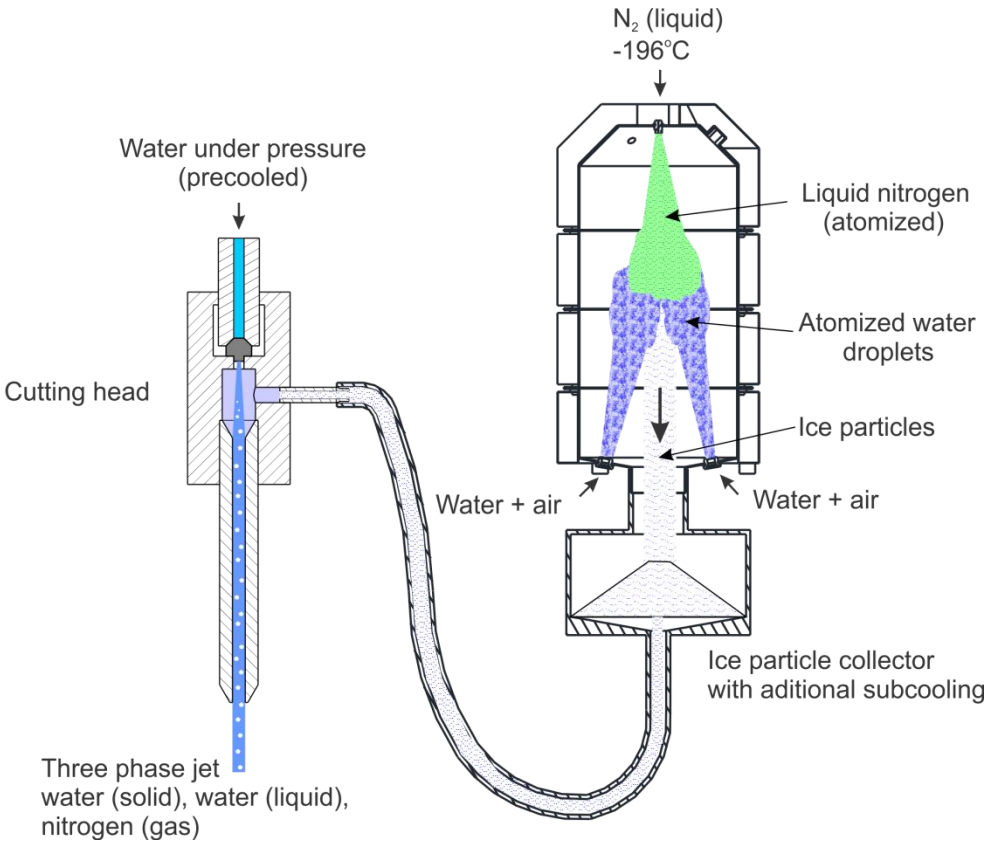

Figure 2: Scheme of the ice particles generation system by atomization and freezing of water droplets [6].

With these processes the goal is to achieve a partial phase transformation of the high speed water jet, that is composed out of water droplets of different diameter ranging from around 100 - 400 µm, into the ice particles. The measured water droplet diameters and consequently the diameters of the created ice particles are comparable to the ones used in mineral abrasive.

However the injection of the liquid nitrogen can also have a negative effect on the jet formation, causing variations in the geometry of the jet. Jet shape and structure is a function of several parameters as density, pressure, water temperature and abrasive particles [7].

Previous experiments in the field of quality of the jet and measurement of the jet diameter have been done by different research groups. Due to possible implementation in industry applications, a quick and easy technique would be useful. Researches [8] have been researching cost efficient methods for measuring the jet diameter using two different component one being a non-contact led micrometer and the other a class 2 lasers. Both methods were effective. Another researches [9] also successfully used a high speed camera

for jet analysis in their research. They took pictures of the high speed water jet to know how the jet diameter changes along its length.

In this research, we want to study phenomenological analysis of the water jet, combining digital image processing with digital manipulation of the photography, and modifying process parameters such as pressure, water temperature and diameter of the water nozzle. In order to verify the effectiveness of this new measurement method, the results will be compared with results from the method that has already been established. Other cutting parameters that will be modified are nozzles, and orifice diameter, water-jet pressure and water temperature.

This method has already been successfully used in previous research [7]. The main advantage is that low cost equipment is required, as well as the result of the jet shape, is get in easy and quickly way.

2 Water jet

The water jet technology is one of the non-conventional machining techniques with growing expectations. The main water jetting technologies used by industry are: WJ and AWJ. The basic methodology is the same. Water is pumped at a sufficiently high pressure, 200 - 600 MPa using intensifier technology like hydraulic cylinders. When water at such pressure is pushed through a suitable orifice (generally of 0.2 - 0.4 mm of diameter), the potential energy of water is converted into kinetic energy, yielding a high velocity jet (1000 m/s).

Such high velocity water jet can machine thin sheets/foils of aluminum, leather, textile, frozen food etc [1], [2].

2.1 Main characteristics of the water jet

Non-traditional machining processes, also called advanced manufacturing processes, are defined as a group of processes that remove material by various techniques involving mechanical, thermal, electrical or chemical energy or combinations of these energies. There are many non-traditional processes such as: chemical machining, electrochemical machining (ECM), electro-discharge machining (EDM), laser cutting, ultrasonic machining (USM) and water-jet technology [10]. In this report, abrasive water jet (AWJ), ice jet (IJ) and cold water jet (CWJ) have been studied.

With these processes the heat is not generated therefore, there is no thermal stress, thermal distortion, or thermal damage. Furthermore the operation does not leave any burr, so no secondary smoothing operation is required. WJ enable fast and precise cutting. Regarding the ecology, the WJ is environmentally friendly process causing almost no pollution. One of the main disadvantages is that a limited number of materials can be cut economically and thick parts cannot be cut by this process economically and accurately.

2.2 Abrasive water jet technology (AWJ)

AWJ cutting is an extended version of water jet cutting. Here the WJ contains abrasive particles such as garnet with high amount of silicon carbide or aluminum oxide in order to increase the material removal rate high above that of WJ machining. Almost any type of material ranging from hard brittle materials such as ceramics, metals and glass to extremely soft materials such as foam and rubbers can be cut by abrasive water jet cutting. The cutting stream and computer controlled movement of the head cutting enables this process to produce parts accurately and efficiently. This machining process is especially ideal for cutting

materials that cannot be cut by laser or electro thermal machining processes. Metallic, non-metallic and advanced composite materials of various thicknesses can be cut by this process. This process is particularly suitable for heat sensitive materials that cannot be machined by processes that produce heat while machining [11]. The schematic of AWJ is shown in Figure 3.

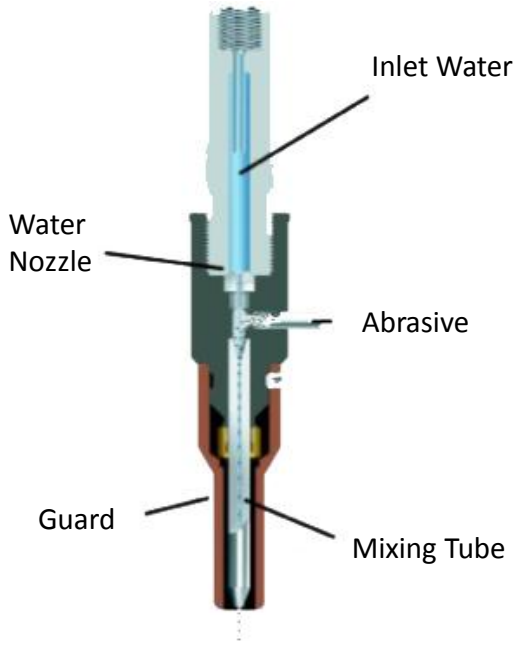

Figure 3: Abrasive water jet machining [11].

It is similar to water jet cutting, but it has some more features underneath the water nozzle; namely abrasive, guard and mixing tube. In this process, high velocity water exiting the water nozzle creates a vacuum which sucks abrasive from the abrasive feed, which mixes with the water in the mixing tube to form a high velocity mixture with the water in the mixing tube to form a high velocity of the abrasives particles [11].

Based on the variety of materials that can be cut, water-jet cutting has already established itself in various industries as an effective procedure for material processing.

Abrasive water jet cutting is used in aerospace, automotive and electronics industries. In aerospace industries, parts such as titanium bodies for military aircrafts, engine components (aluminum, titanium and heat resistant alloys), aluminum body parts and interior cabin parts are made using AWJ cutting. In automotive industries, parts like interior trim (head liners, trunk liners and door panels) and fiberglass body components and bumpers are machined by

this process. Spelling, in electronics industries, circuit boards and cable stripping is made by AWJ cutting.

2.2.1 Advantages and disadvantages of AWJ

A decisive advantage of the WJ and AWJ cutting process is that it is a cold process [12]. No high temperatures that could cause microstructure changes, edge zone hardening or micro-cracks affect the cutting zone. The AWJ creates a very small cut width. The cut edges are of astonishingly good quality and require a costly reworking only in the rarest cases. High material prices and limited raw material resources demand optimal usage of resources. This created an important economic argument for water-jet cutting.

The high-pressure WJ can never get jammed in the cut width. Since the WJ has a very high power density and therefore the cutting head can be built very compactly, the process has good accessibility. Another essential advantage of the process is that the material removed from the cut during the cutting process, is flushed by the water.

Limitations of abrasive water jet cutting are: it cannot cut materials that degrade quickly with moisture. Besides, surface finish degrades at higher cutting speeds which are frequently used for rough cutting. It demands high capital costs and yields high noise levels during operation.

Despite the high kinetic energy of the water-jet, there is as good as no deformation in the material and a high cut precision is achieved without or with only minimal fraying and burring. In combination with the high traverse speeds, it is thus possible to process softer materials such as seals or foams extremely well [12].

2.2.2 Influencing parameters

The results of AWJ cutting quality are affected by different parameters of the water jet and of the work piece [12]. Relations between AWJ process parameters are shown in figure 4.

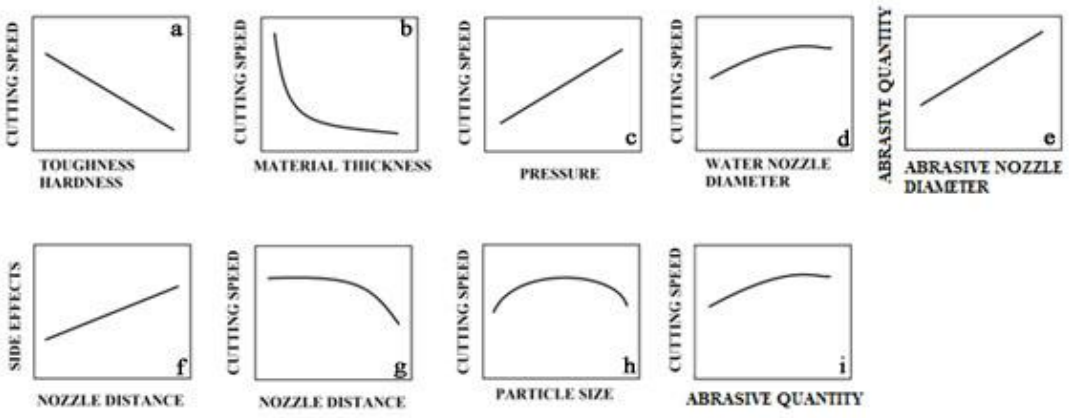

Figure 4: Parameters more representatives about work piece [12].

The feed rate of the machine will be determinate for strength and hardness of the work piece. The harder the material is, the slower the cutting speed (Figure 4.a); the quantity of the cutting material depends directly of the thickness of the work piece. The greater the thickness of the material to be processed, the slower the cutting speed, since with equal feed more material must be removed (Figure 4.b); it is not only the maximum depth of the cut that depends on the pressure; with increasing pressure, it is also possible to increase the cutting speed and achieve the same cut results. The dependence is almost linear. With increasing pressure, however, the wear on the pressurized parts increases and process stability decreases (Figure 4.c); the diameter of the focusing nozzle can be increased to get a higher cutting speed, however, not without limits. The hydraulic power increases, which means higher power consumption of the pump. Moreover with increasing jet diameter, the cut width becomes larger; this means that more material must be removed (Figure 4.d).

The larger the diameter of the water nozzle, the larger the diameter of the abrasive nozzle must be. With increasing diameter of the abrasive nozzle, the quantity of abrasive to be added must be increased (Figure 4.e); increasing the distance between the abrasive nozzle and the work-piece causes a decrease in the cutting speed due to the associated jet divergence. At the same time, the cut width increase and the sand blast effects close to the cut cause secondary damage on the top of the work-piece (Figure 4.f); the selection of the nozzle distance is very important, the smaller the nozzle distance, the higher the cutting speed and therefore the smaller the damaging side effects. In practice, a constant nozzle distance of approximately 1mm should be adhered to (Figure 4.g).

The material removal depends on the type, particle size and quantity of abrasive. The harder and tougher the abrasive is, the faster the cutting speed. The larger the abrasive particles are, the faster the cutting speed. With decreasing particle size, the cut quality

increases (Figure 4.h); for each nozzle combination, there is an optimal abrasive quantity. If you increase the quantity, the cut speed increases constantly until the optimum is reached. The smaller the pressure fluctuations and thus the speed difference in the water-jet the faster the final speed of the abrasive particle. The same also applies to fluctuations of the added abrasive quantity. In both cases, fluctuations that are too large cause, among other things, blockages and friction losses and they thus decrease process stability (Figure 4.i).

2.3 Ice Jet technology

Ice Jet technology (IJ) technology is a non-destructive, non-abrasive, residue free, and environmentally friendly way of machining. The use of ice particles instead of mineral abrasives solves problems of abrasive waste management [1].

The hardness of ice particles which is between 1.5 and 3 Mohs depending on the temperature and size, is less than that of abrasive particles used in a conventional AWJ machining[1]. Thus, the expected productivity of IJ is less than the productivity of AWJ. Nonetheless, the feasibility to shape contamination sensitive materials and the elimination of the negative environmental effects makes this loss of productivity acceptable. The main drawback of IJ machining is the difficulty to generate and handle the ice particles.

To better understand the processes that occurring in IJ formation it is necessary to first understand some basic physic of water ice like [1].

Elastic is an important ice feature determining particle behavior in the course of impact is ice elasticity. At the temperature range of -3 ºC to -40 ºC, ice behaves as almost perfect elastic body. The adhesion and sintering is one of the main issues in the use of ice particles to the surface of the enclosure. Its solution requires a fundamental understanding of the physical mechanisms of bonding between ice and other solids. In particular, it is very essential to find out the nature and strength of molecular bonding between ice and other solids. The strength of the adhesion of ice particles depends on the ice temperature.

The sintering is the process of vapor diffusion which joins individual ice grains together to form an ice skeleton of connected grains. The eventual effect is a stronger snow layer. It is necessary to maintain ice temperature below -30 ºC to prevent sintering of ice particles. The sintering is also determined by the duration of the particles contact.

The adherence of the ice to walls or sintering of ice particles is caused by the moisture contained in the atmosphere in the course of ice transportation. Both phenomena result in the formation of a plug and clogging of the conduits [1].

The strength of the adhesion of ice particles decreases rapidly when system subjected to the temperature below -15 ºC. Therefore, it is very important to monitor the temperature of ice particles on the outlet (control point) of IJ system.

According to the equation 3.3,

$$\rho = 0.9152e^{(-0.0001T)} \qquad (3.3)$$

where ρ is the ice density and T is the ice temperature, is established the functional dependency of the ice density [1].

2.3.1 Ice jet generation by entertainment of sub-cooled ice particles

Technology that uses entertainment of sub-cooled ice particles for IJ generation works in the similar way as AWJ, with the difference that instead of mineral abrasives it uses pre prepared sub-cooled ice grains. Schematic depiction of such a system is presented in Figure 5.

The ice grains are injected into the cutting head in much the same way as mineral abrasive is, using the Venturi effect. Because ice grains are generated in advance, their size, shape and temperature can be controlled, allowing us to create ice particles with maximum hardness.

Figure 6 shows Brinell hardness function as a function of ice temperature. From the plot we can see that the hardness increases as the temperature of the ice decreases, therefore it is very important maintain low.

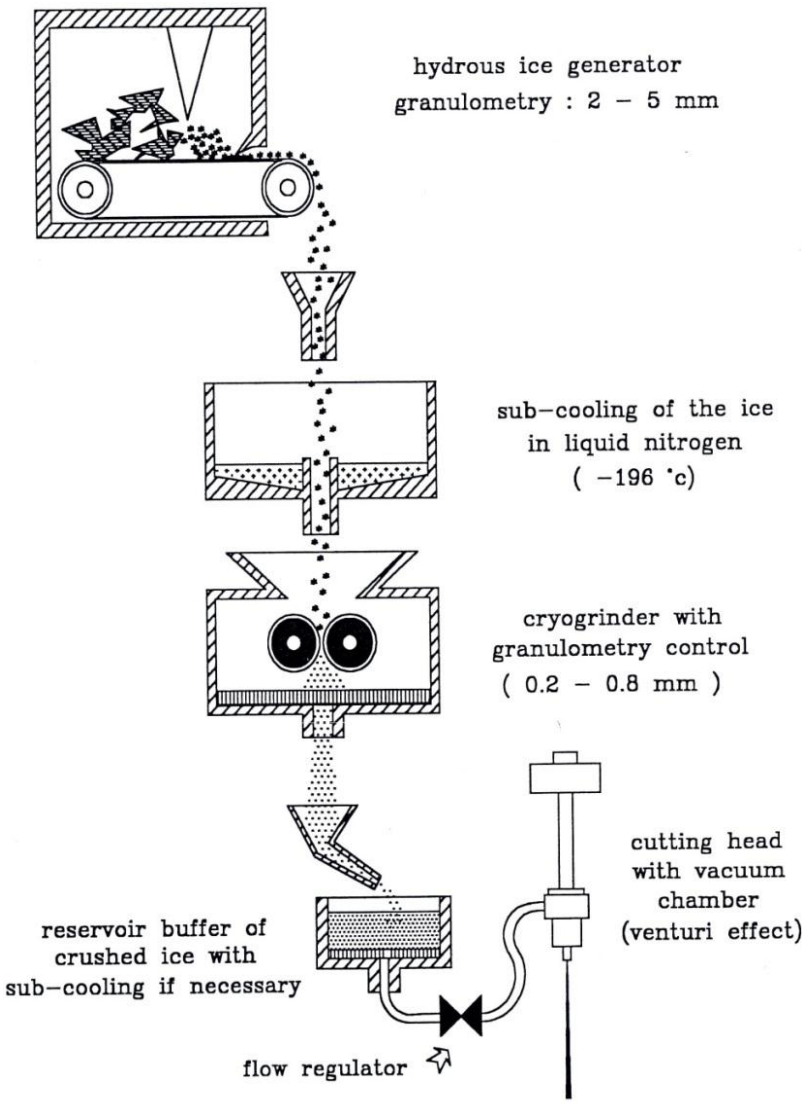

Figure 5: Schematic depiction of ice particle generation and transportation system for IJ machining [14].

The main downsides of this method are such as, these systems require additional space and they use up a lot of energy for transporting of ice particles to the cutting head, because of they come in contact with the surrounding air and friction heated high speed water in the mixing chamber of the cutting head.

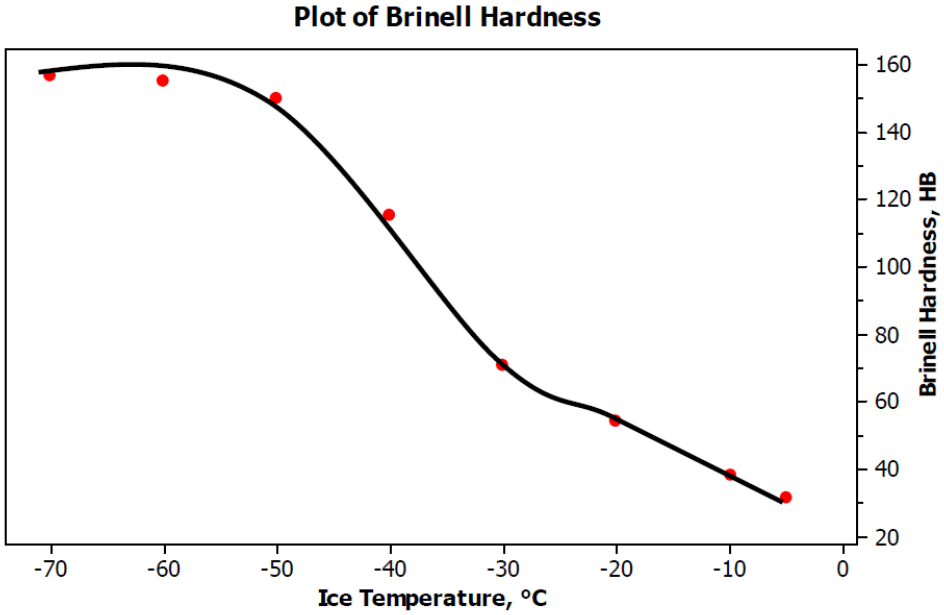

Figure 6: Brinell hardness as a function of ice temperature [1].

The time it takes to warm up the ice grain with diameter 0.1mm, from the temperature of -194 ºC to 0 ºC is [1]:

- 8 x 10^{-2} s on the air of 20 ºC.
- 2 x 10^{-4} s in water of 40 ºC.

The time it takes for the ice particle to travel the distance to the work piece is in the same order of magnitude, but was proven that such a process is feasible.

Method for IJ generation by entertaining sub-cooled ice particles prepared in advance shows much promise as it allows us to control the important process parameters such as ice particle granulation and temperature. The main problem facing the researchers is the creation of economically acceptable system that efficiently generates stores and transports ice particles to the cutting head [1].

2.3.2 Ice jet generation by super-cooling of pressured water

This method of IJ generation uses thermo dynamical properties of water for in situ ice particle generation during the formation of the water jet itself. That can be achieved by the use of cryogenic or liquid gases, and a heat exchanger to cool down the high pressure water [1]. The process is shown in Figure 7.

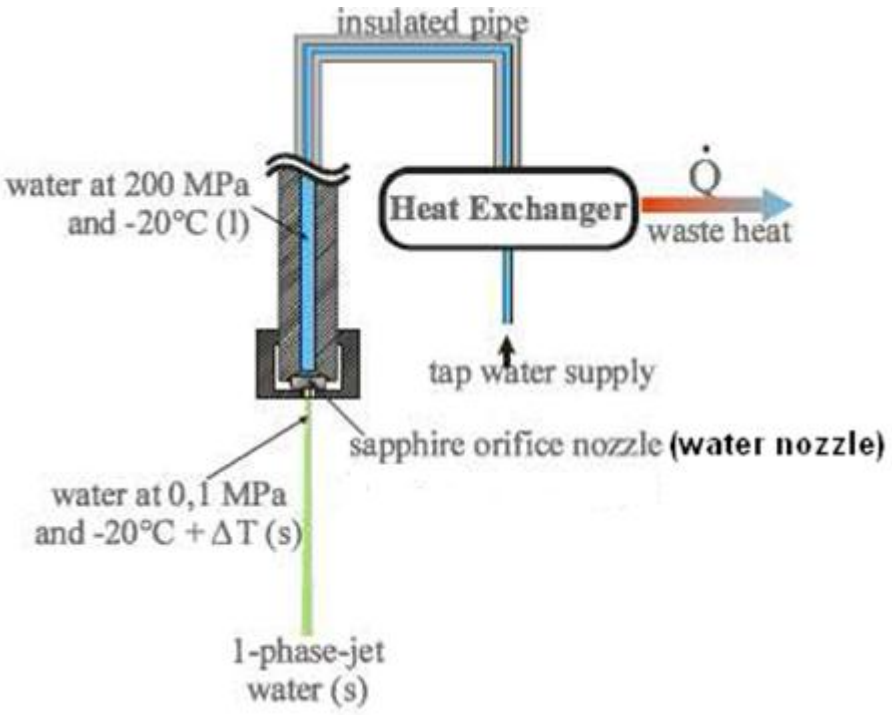

Figure 7: In situ Ice Jet generation by super cooling the pressurized water [15].

The water at normal atmospheric pressure has a freezing point at 0 °C. As one can extract from the phase diagram of water in figure 8 with the magnified zone of interest, this is not the case at the pressure of 200 MPa. Under these conditions, the freezing point drops down to -20 °C. It can then be transported to the water nozzle, where the potential energy of the high pressure water is transformed into the kinetic energy. Due to the pressure drop at the water nozzle exit, some of the water instantly changes its phase from liquid to solid, forming the IJ [1].

Properties of different types of ice vary, but for practical uses, the most important type of ice is Ice I. The important feature of water is the reduction of a melting temperature with the increase of pressure as can be seen in Figure 8. The minimum temperature of the liquid water is attained at the pressure about 200 MPa and is equal to -20 ^{o}C. The reduction of the water solidification temperature from 0 ^{o}C to -20 ^{o}C as the pressure rises from 0,1 MPa to 200 MPa is almost linear [1].

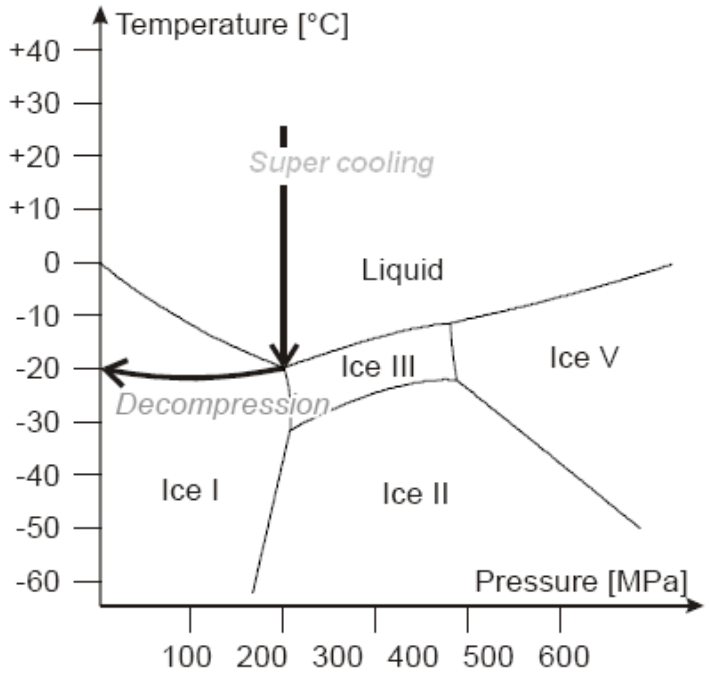

Figure 8: Phase diagram of water with the magnified zone of interest [14].

Problem with this method is the difficulty to control the generation of ice, as this process is inherently random and poses instability in the process.

2.3.3 Ice jet generation by freezing of the water-jet

Method of in situ IJ generation by freezing of the water jet inside the mixing is based upon the extreme high enthalpy of evaporation of cryogenic liquefied gases such as CO_2 (-78.5 °C) and N_2 (-195.9 °C). This enables a massive heat transfer from the water to the gas and a subsequent partial of the high speed water jet phase transformation in the mixing chamber and the focusing nozzle. Method is depicted in Figure 9.

In this method ice particles are formed inside the mixing chamber, as a result of contact with a cooling media and are then accelerated by the high speed water jet. Because of the high speed and coherence of the water jet, the generated ice particles are mostly frozen water droplets from the dispersion of water around the main water jet which has a lesser speed.

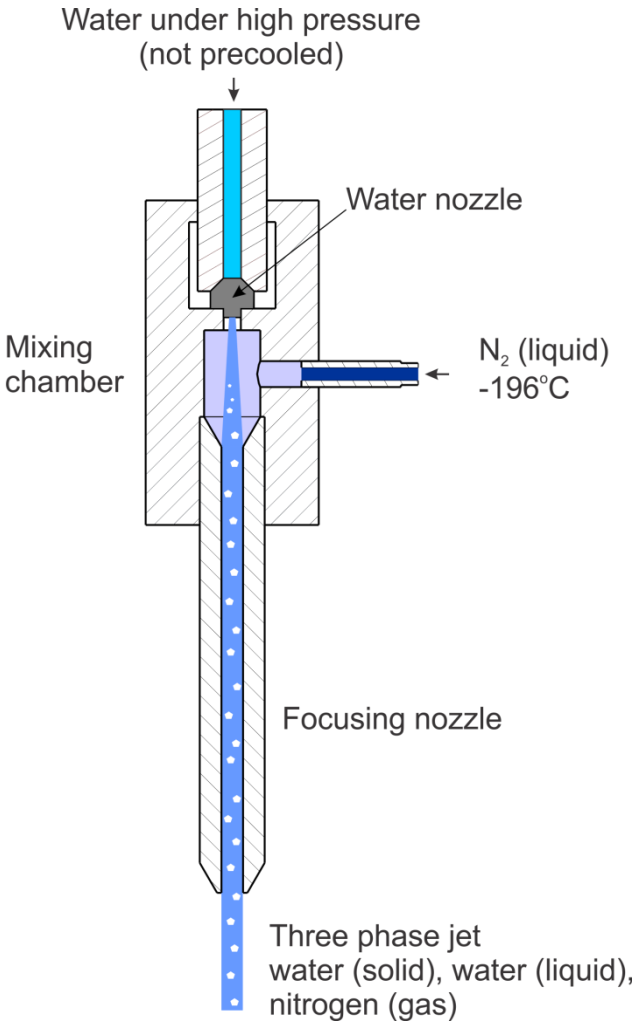

Figure 9: Ice jet generation by freezing of the water jet inside the mixing chamber [6].

Particle formation must be fast enough because of the short distance of the work piece and very fast water jet speeds and must also be constant ice particle formation inside the mixing chamber and focusing tube of the cutting head [6].

There is a problem regarding stability of created ice particles because of the heat of the water jet and the temperature of the created ice particles which greatly affect their hardness. Furthermore, the low temperatures introduced may also affect the durability of the standard AWJ equipment used, such as the water nozzle and the collimation tube that were not designed to operate in this environment [15].

The ice generation by freezing of the water jet method needs the least amount of space for extra equipment and promises to be the least power consuming.

3 Methods of water jet spread measurement

Water jet is limited technology by poor accuracy in comparison to other machining processes like laser, wire electro discharge machining or milling [16].

The problem lies in the geometrically non-defined and flexible tool as it has a multiphase structure and it disintegrates in the air atmosphere, which is difficult to analytically analyze. Another source of inaccuracy is the specific surface texture and tapered cut which is characteristics for this type of process. While there is no present solution for the surface, the taper problem is currently solved by tilting the cutting head. Other significant problem is also determining the dimensions of the diameter of the AWJ as these data are used for setting the tool offset while cutting. Currently this is done by using the radius of the focusing tube as a tool offset. While this is good for when the focusing tube is new and if we are satisfied with the accuracy up to ±0.1mm, it is not good after the tube starts to wear or we want to achieve machining accuracies less than ±0.1mm. That is why a method is needed which would measure the AWJ diameter at the stand-off distance from the nozzle exit [17].

To get a better accuracy in measurement several methods for the measurement of the characteristics of the aqueous jet have been developed. Based on the presented methods, one will be chosen and used in practice.

3.1 LDV Method

LDV (Laser Doppler Velocimetry) is a method, which uses the Doppler Effect revert for the measurement of the direction and velocity of liquids. The measuring system is given by a monochromatic source of light. Laser beam is focused in the ray towards the measuring object and covers the reflected radiation. The change in wavelength of the reflected beam is a function of the relative speed of the measured object.

3.1.1 Development

With the development of the He-Ne laser in Bell's laboratories, in 1962, the scientific society got a device which assured a constant electromagnetic radiation with a wavelength of 632.8 nm (red light of the visible specter)[18]. Soon afterwards, it came up that it is possible to perform the measurement of a liquid with the use of the laser and tiny polystyrene beads in a liquid through the Doppler Effect.

The first LDV system had been developed by Brown laboratories.

3.1.2 Description of the method

In the basic version of the LDV method, given in Figure 10, monochromatic source of light (laser) was used. The ray is divided by the optical system, which assures the coherence beams. Normally we use lasers with a wavelength in the visible specter (390 - 750 nm), which permits the observation of the ray. These two rays consequently divide in their focal point, which is in this example in the spot of measurement and forms individual interfering lines, perpendicularly to the direction of the observed liquid. If a particle, finding itself in the liquid spontaneously or artificially, crosses the measuring point, reflects the light which is detected, taken in by the photo detector [18].

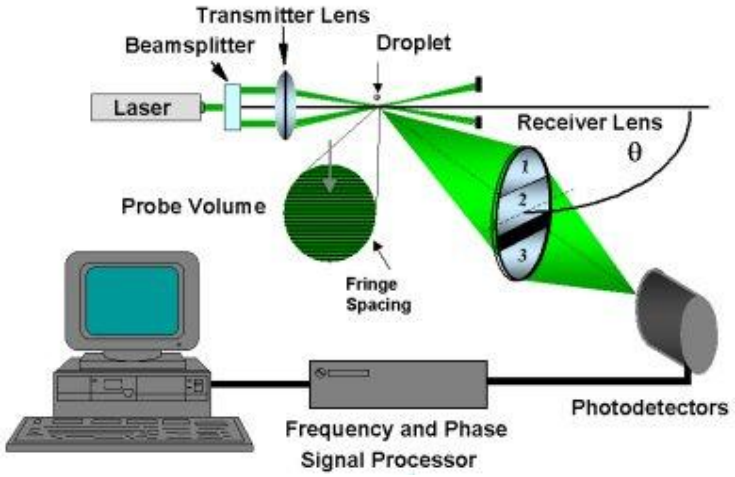

Figure 10: Simple LDV [18].

Intensity and frequency of the reflected light fluctuate. This event is described as the Doppler Effect. If the sensor is put in such a way that the interfering lines are perpendicular to the direction of the liquid, the electric signal from the sensor will be proportional to the whole speed of the particle (marker), we get along the speed of the liquid flow too.

The marker permits the use of LDV in practice and has a similar density as the observed liquid; at the same time, its reflectance factor is different from the factor of the liquid. The particle can be given by a special type of plastic, polystyrene, aluminum gravel, glass beads, etc. The marker has to be big enough to reflect an adequate quantity of light. The size of the markers is in the range 10-100 micrometer, depending on the type of liquid. In case the particle is too big, it could affect the flow of the liquid, which is unacceptable. LDV technology is no-contact method and it has a high frequency of response.

However is necessary a good transparency between the source of light, the aimed surface and the photo detector and the precision of the measurement depend on the adequate setting of the sent and reflected ray. This technology has an expensiveness of the instrumentation.

3.2 PIV Method

The method PIV (Particle Image Velocimetry), given in Figure 11, is an optical method of visualization of the flow. It I used for measuring the vector of velocity of the marker and the characteristic of the liquid itself. An important difference between the methods LDV and PIV I the fact that with the latter we get a two –dimension or 3D vector field, while in case of the LDV we measure the speed in only one point. Both the methods are similar, we can think of the PIV as the upgrade of the LDV.

Similar is also the PTV (Particle tracing velocimetry) method: smaller number of markers, a single particle can be observed; and the LSV (Laser speckle velocimetry) method: higher amount of markers makes it impossible to observe a single one [16].

3.2.1 Description and composition of the PIV system

As in the method LDV, also in the PIV one crucial parts of the measuring system are the markers (particle, tracer particle). The size of a particle in the range 10 - 100 micrometers assures that the particle is small enough to respond properly to the change in the flow of the liquid and still big enough to reflect an adequate quantity of light.

The receiver of light is in this method a camera or, nowadays, a CCD chip. The difference is primarily the fact that the analysis is less clear with the camera, for the analysis we use one picture and from it, through the use of auto-correlation, define the flow of the liquid. Consequently, due to auto-correlation, from the picture it cannot be noticeable which marker comes from the first impulse and which one from the second. From this point of view, the use of the CCD chip is preferable, because, at high speed, we are able to take two pictures in the interval of a couple of nanoseconds, which is more useful for a more precise analysis of the liquid flow. The lack, or limit, of this kind of cameras is the fact that they record only two pictures in such a short period of time and before they are able to record two new ones it is necessary to transfer the first two ones to the computer, where they wait for further treatment [16].

According the strength of the used laser, we differentiate the macro end micro PIV, the latter is used for the measurement of micro-flows. For a macro configuration the Nd : Yag lasers are used, since they have a capability of transmitting high-strength rays in short

impulses. These lasers transmit a wavelength of 1064 nm and its divisors of a wavelength 532 nm, 266 nm, etc. Due to safety reasons, a special filter is used at a wavelength of 532 nm which blocks this wavelength since it's the only one visible with the eyes (green visible specter). Optical fibers are used to lead the ray to the calibration system. Through the use of a cylindrical lens, the ray is spread into flatness, and is made thinner through the use of a spherical lens. Thanks to the combination of a cylindrical and spherical lens, the measurement of the speed vector is assured.

For the coordination of both cameras or more of them, a synchronization unit is used. We know the digital and analogue performance, the latter is quite old fashioned and its used is abandoned. Most of systems are digital, since the controller controls, through the help of the computer, the CCD camera and the laser at 1 ns of precision. Knowing the precise time of triggering, in the PIV method, is of great importance, since it permits the determination of the liquid speed.

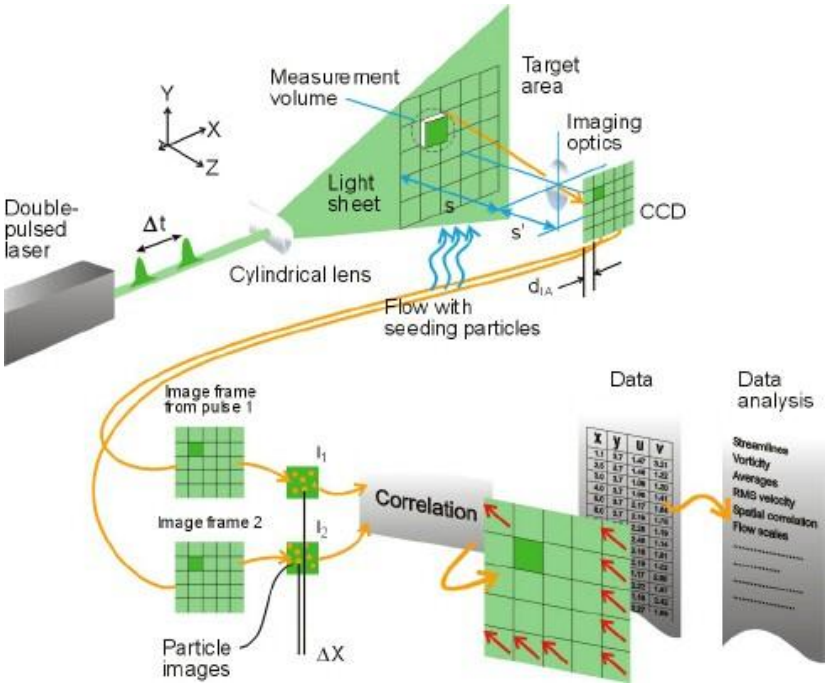

Figure 11: Example of measurement with the PIV method [19].

As advantages of PIV method are, measurement in a multi-dimensional space, comparison of recorded pictures in the real time or later, displacement of individual points permits a high level of precision (10% pixels) and PIV is no contact method.

In the other hand, in some occasions it is difficult to determine adequate markers, that would completely follow the movement of the liquid, in most of methods, the measurement in the Z axis (the side towards the camera) is not possible. The result of the measurement is a

special average approximation of the real value and the use of an IV grade laser is necessary as well as the one of a speed camera, and this is the reason why these systems are quite expensive.

3.2.2 Other frequent forms of PIV

From the basic PIV method also other methods have been developed, more complex derivate of the original form. Some examples are presented further.

3.2.2.1 Stereoscopic PIV

In this case, two cameras are installed with a different point of view to permit the determination of the z-axis shift. Both cameras are focused on the same spot in the liquid (Fig. 12). The most precise setting is achieved when the angle between the cameras is 90°.

Stereo PIV uses a similar principle as person's eyes. Each of our eyes sees a slightly different view which is transformed in one single picture by our neurons. If we observe the world only with one eye, we are hardly capable of determining a feeling of space (distance and movements away from and towards the eye), while the movements up, down, left and right are normally detected with one eye only. Consequently, we can state that the cameras function as our eyes [20].

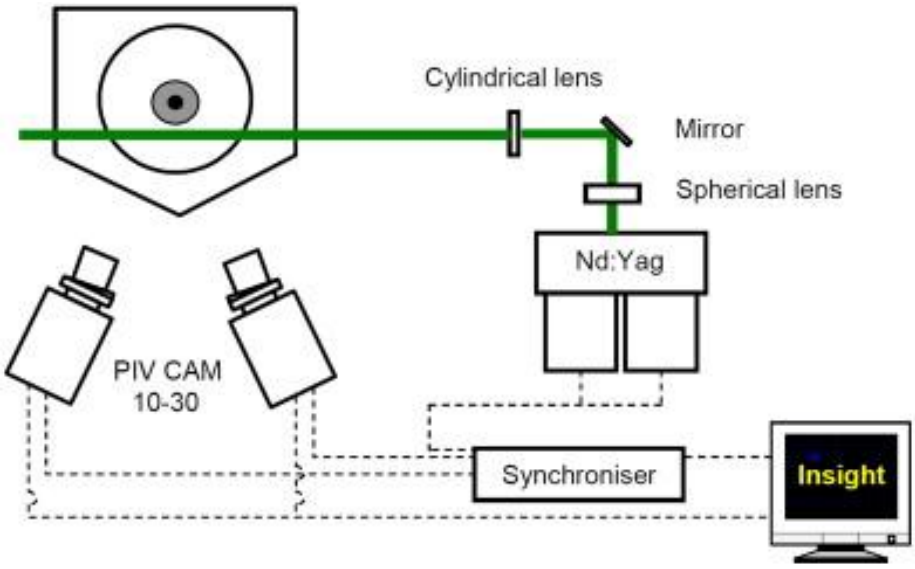

Figure 12: Presentation of the stereoscopic PIV method [20].

3.2.2.2 Micro PIV

Microscopic flows are analyzed through an epifluorescence microscope. An important issue in this method is, that the fluorescent particles in the liquid excite at some wavelength, and emanate at another one. The laser light is reflected thank to a dichromic mirror and

pointed through the lens, where it is focused on the observed point. The emission of the particles light, along with the reflected laser light, passes through the diachronic mirror and through the filter emission, which blocks the laser light. Differently from the PIV, where the characteristics' analysis is given in two dimensions, in the micro PIV due to the characteristics of the lens we can focus on only one dimension. A simple example of micro PIV is given in Figure 13.

The particle size is in the range from some nanometers to some micrometers. They must be big enough to amortize the appearance of Brown's shifting (when the particles do not follow the flow of the liquid).

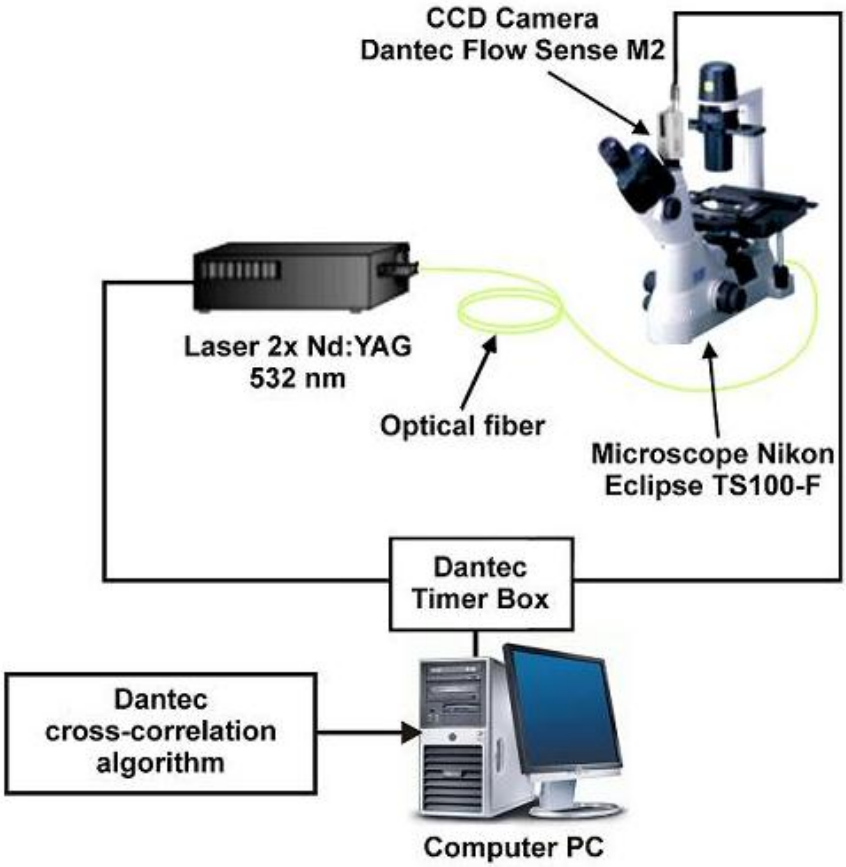

Figure 13: Example of micro PIV representation [21].

3.2.2.3 Holographic PIV

The method extends on different experimental methods, which use interference coherent particle's light in the liquid and a ray of reference to obtain data about the amplitude in phase of spread light at the level of the sensor. The obtained data, also called hologram, is used for the reconstruction of the initial intensity of the space. This goal is achieved in a way to

illuminate he hologram with the ray of reference, thank to optical methods or digital approximations. The picture can be recorded on photographic film or with a digital camera, from which it can be immediately transferred to the computer. The advantage of this method is the possibility of a hologram sequence that provides the liquid flow in 3D [16].

3.3 PSV method

This is a variant of the PIV method. The main difference between them is in the fact that, in the PSV method, a weaker source of light is used, a led diode, while in the PIV method, a monochromatic light source-laser is used. Both methods are presented in Figure 14.

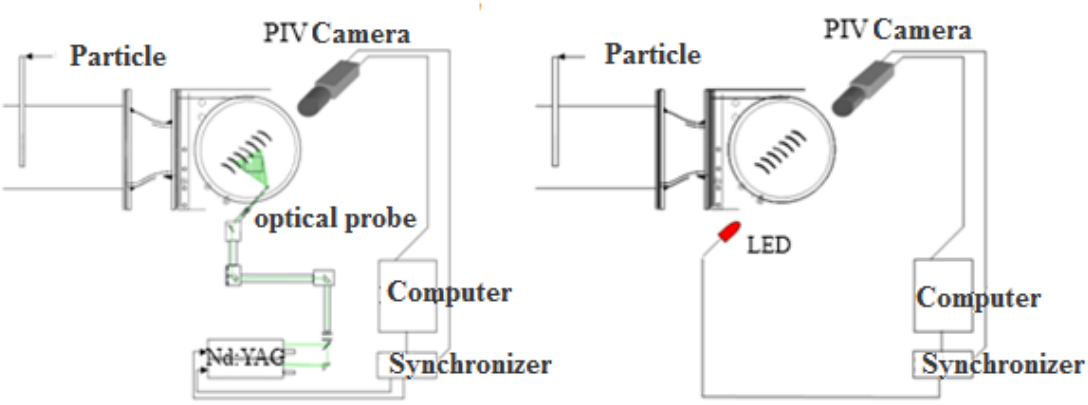

Figure 14: Presentation of the measurement system PIV (left) and PSV (right) [22].

3.3.1 Description of the PSV method

LED diodes are used as light sources; their advantage is primarily in the fact that they are capable of fast pulsing and are relatively cheap. There are different mono-colors which provide the recording of a multi-color picture, which is not possible when a laser is used. The measuring system permits the setting of the working distance (WD), field of view (FOV) and depth of focus (DOF). The exact setting of the DOF is important primarily to assure a precise particle result, which are of our interest. The particles that are in the focal level provide the darkest shadows. Other particles, which do not interest us, are removed during the measuring. The performance of the measurement is equal in the PSV and PIV method (CCD chip, computer). The picture obtained with the PSV method is a negative of the picture obtained with the PIV method.

The PSV method is very useful when dealing with liquids that have bubbles. The PIV method does not permit it, because the recording of the bubbles and oxygen is difficult, since

it an error can occur easily (the laser light reflects itself in different directions when bouncing into a bubble; the illumination of bubbles that are not at the focal level can happen). There is no such problem in case of PSV, since we do not rely on the shadow of the bubbles, which appear on direct illumination.

In practice, also a derivative of the PSV is used, which differentiates from the basic form for the interrelation of the observed flow, light source and measurement detector. This method is named Side Scatter. The most noticeable difference is the illumination of the picture, the individual pictures are the negative one of another, which is the consequence of light reflection and shadow throwing.

The low price of the components (primarily of the light source) and quite precise and simple method are the mains advantages of PSV method.

However lower picture quality, providing of only the particle speed and long processing of the pictures are the mains disadvantage.

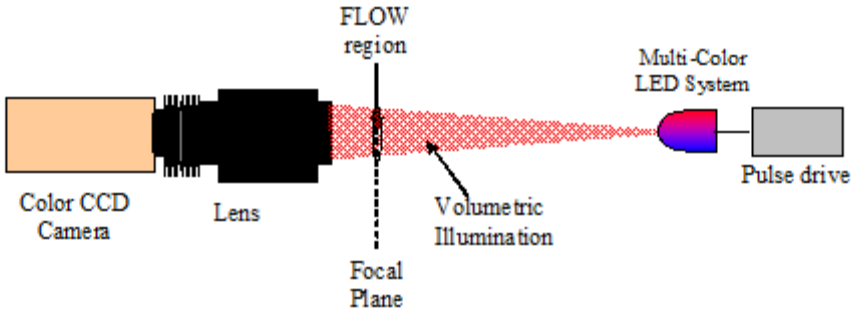

Figure 15: Example of a PSV measurement system [22].

3.4 L2F and LIF methods

Both the methods are of no-contact and are rarely used for the measurement of the aqueous jet, this is why they will be just shortly described. Primarily an interesting LIF method is possible, that has a big potential for further development, since we will use in the future even more computer technology. The LIF method could possibly develop in the future into a more accessible and automated method.

3.4.1 L2F

Two foci laser anemometry is in its basic form an optical pointing measurement through the use of a laser, similarly to the before mentioned LDV, or LDA. The measurement principle is thought of in a way to project two points on the distance of 250 micrometers in

the field of the liquid. The density of the points themselves permits the observation of smaller particles than in case of the LDV method. The disadvantage of this method is in the fact that the measurement itself is more vulnerable and/or imprecise when measuring turbulent flows [16].

3.4.2 Laser induced fluorescence (LIF)

The LIF is a spectroscopic method used for the determination of molecular structures, measurements and the visualization of a liquid flow. To obtain the excitation of the measured space, a laser is used. The wavelength is chosen in a way to assure it has the highest section with the particle. The excited particle obtained, settles in a very short time (some nanoseconds) and afterwards, emanates light, whose wavelength is higher than the excitation one. The obtained fluorescence light is measured with a special photo tube PMT.

3.5 Photographic method

For the capturing of the visible part of the light we can determine the characteristics of the jet, until a limit. For such capturing a high-speed camera is used, a photo camera, where a short time of the diaphragm is set which assures a quite sharp picture.

In case of this method we know more configurations if the measurement system itself. Usually the illumination body is set on the camera (Figure 16). Nevertheless, sometimes better results are obtained with a setting where the source and the detector are at opposite sides of the observed object. For the illumination from behind, the appearance of a sensor saturated with light is often, since the light, through the object, illuminates straight the detector.

Simplicity of the system and relative affordable are the main advantages of photographic method. However, the main disadvantages are two, provides only the shape of the jet and weak contrast between the mist / spray phases.

Figure 16: Example of a high-speed camera [23].

3.6 Method with the use of infrared photography (IR)

This method is in practice relatively rarely used, but still permits, due to the characteristics of the NIR (near infrared), a good insight in the development of the jet, and, differently from the classical method of photography, clearly differentiates the core of the jet and the transmitted mist. In this context it is important to point out that it is true only for the NIr, not for the thermal photography.

The water is a colorless liquid, which is impermeable to the visible specter of light. Due to aerodynamic friction, the superficial layer of the jet splits and encloses with the mist, which spreads the light and makes the treatment of the picture more difficult. In case of IR specter the matter is the opposite, water completely absorbs the IR part of the light, the mist permeates it partly, while air totally permeates the IR light. In the translucent method, where the source of light is set in front of the optical detector, while between them there is the observed jet, it applies that the core of the jet doesn't permeate light, and this is the reason why it is quite dark in white-black picture, the mist has a shade of grey, and the rest (air) is light. In case that we put the camera and the detector on the same side of the jet, we can also get good results, the only difference is in the fact that the colors in the black and white picture substitute.

For the described method the use of IR specter of light is necessary. A problem comes up when the human eye detects wavelengths of light around 600 nm, because the IR zone starts up from 700 nm. Due to the fact that most of the used detectors are used to detect the visible

specter, IR photography need some special components. For the photography itself it is best to use a special film and an optical filter to remove the visible specter. The latter is necessary, since the film is sensitive to visible light.

In the digital era, special films are not needed anymore. The CCD and CMOS sensors installed in the digital cameras themselves are physically capable of detecting wavelengths over the visible specter, somewhere around 900 nm, depending on the sensor. This is still not the 'real' IR light, but it finds itself in a range near to the IR one. Due to the fact that a distortion of the picture can occur as a consequence of the IR light and due to legislation, all the sensors have on them filters, that to not let the IR specter pass through. Legislation is rather strict and precise and prohibits IR photography, besides in case of research goals. Before the prohibition, there were quite a lot cameras produced in batches without filters (Figure 17), nowadays, a physical intervention on the machine and the removal of the filters from the sensor is needed to obtain a camera without a filter.

Figure 17: Example of a camera for IR photography Sigma - SD14 [24].

Due to the fact that sensors are sensitive to the intensity of the incoming light, regardless the wavelength, for IR photography a filer is necessary, that does not let visible light pass through. A problem comes up because the CMOS/CCD sensor is designated to the visible specter and RGB (red, green, blue) detectors saturate with visible light. Through the use of the filter, that does not permeate wavelengths above 650 - 700 nm, we permit to the IR specter to get to the detector. Its location in the measuring system is generally arbitrary, and the use of more filters at nce is also possible. If the record isn't taken in the darkness, visible light is also present, and this is the reason why the filter has to be set somewhere in the camera (as the lens itself or on the lens). In the translucent method, the problem of saturation

of the sensor with light can show up. It is valid especially, if the source of light is too strong or wide, and the intensity of light getting into the sensor is too high. The phenomenon of saturation is quite often in case of the translucent method. Depending on the location of the filter in the system, in most cases, any source of light is acceptable, when it reflects NIR light, but it is not limited to that specter only.

Only the picture opposite to the expectations has no red shades. Modern sensors use the RGB signaling interpolation, to fulfill the gaps between the individual detectors; besides that, IR light excites trough the 700 nm filter all the detectors, though not the red ones. Often appear shades of violet color. To remove this kind of effects, it would be necessary a strong intervention on the camera's processor and the change in the polynomial interpolation. The best thing to do is to transform the pictures into black and white ones; to guarantee a better quality of the results it is advised to filter the interferences. For the capture of the picture of non-coherent jets a short illumination is of great importance, where the method is comparable to high-speed photography: the time of illumination is crucial.

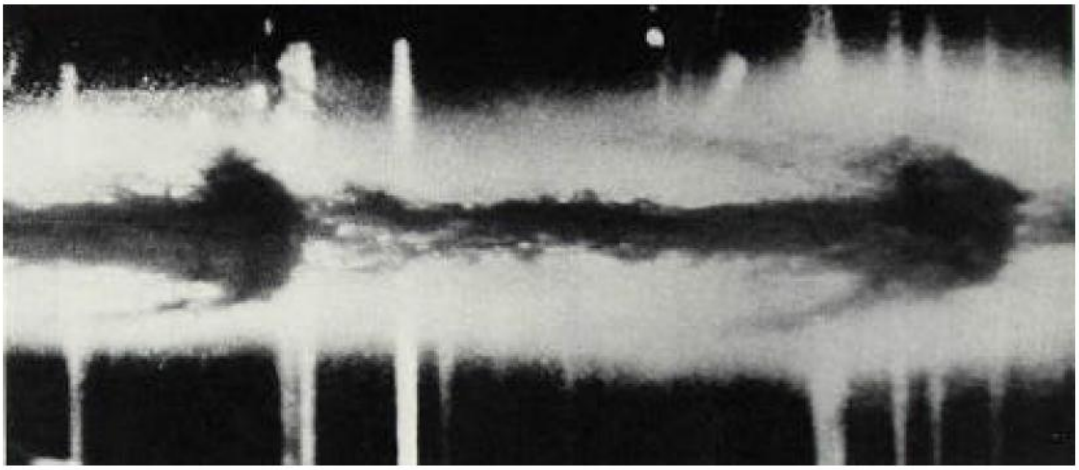

Figure 18: Example of IR photography of an impulse jet [25].

Optimal contrast between the phases of the jet, relatively acceptable price and quite simple method are the mains advantages.

However, it is necessary a special camera and only the speed of the jet is obtained.

3.7 Cantilever load cell method

The measuring system consisting of a load cell and a wear resistant probe has been developed [17]. The device measures the force of the jet while it passes over the edge of the probe. If the feed rate of the jet is constant and the time needed for jet to pass is known, the diameter can be determined.

3.7.1 Description of the method

The configuration of the device for measuring the diameter of the jet is shown on Figure 19. The device consists of a load cell with a fixed wear resistant probe. The cell is assembled through a fixture on the AWJ machine catcher wall. The load cell Vishay Transducers 1022 is a cantilever type of a binocular shape intended for measuring of axial forces. It has an IP66 protection against dust and moisture and can measure maximum loads of 7 kg at the rated output of 2.002 mV/V and total error less than 0.02%. The compensated temperature range is between -10 and 40 ºC. The probe has to be made of hard material with well-defined edges. This is why a carbide insert used for turning was employed.

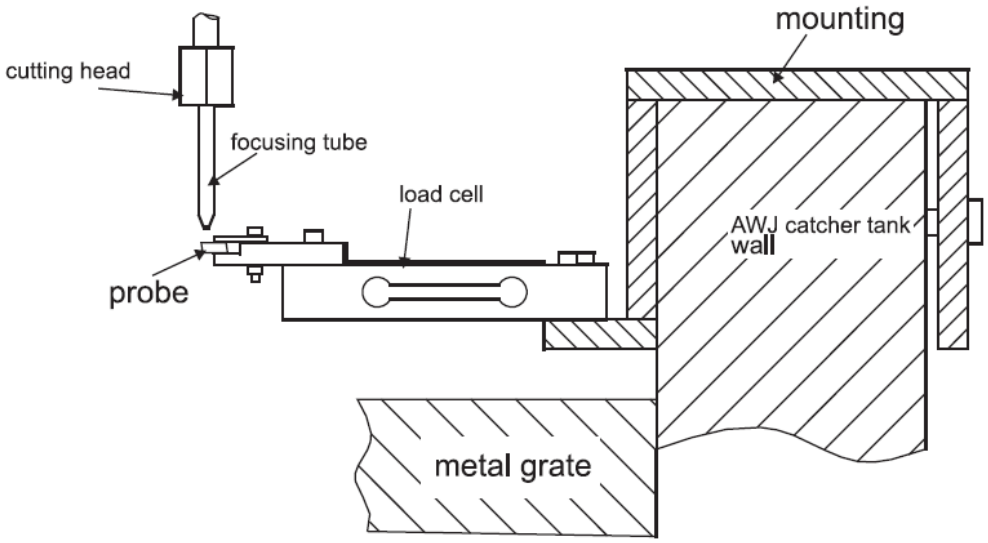

Figure 19: The configuration of the jet diameter measurement device [17].

The measurement method for defining the jet diameter was conceived so that the impact force of the jet would be measured while it passes over the edge of a probe mounted on a load cell as it is shown in Figure 20. The jet is moving with a constant velocity "v" and when it touches the probe, the measured force starts to rise. When the whole diameter of the jet has passed over the edge of the probe the force ceases to rise. If the time "t_d" when the force starts

and when it ceases to rise is known, the diameter of the jet “d” can be determined by multiplying the time with the traverse velocity of the jet (Eq. (4.7.1.))

$$d = v * t_d \qquad (4.7.1)$$

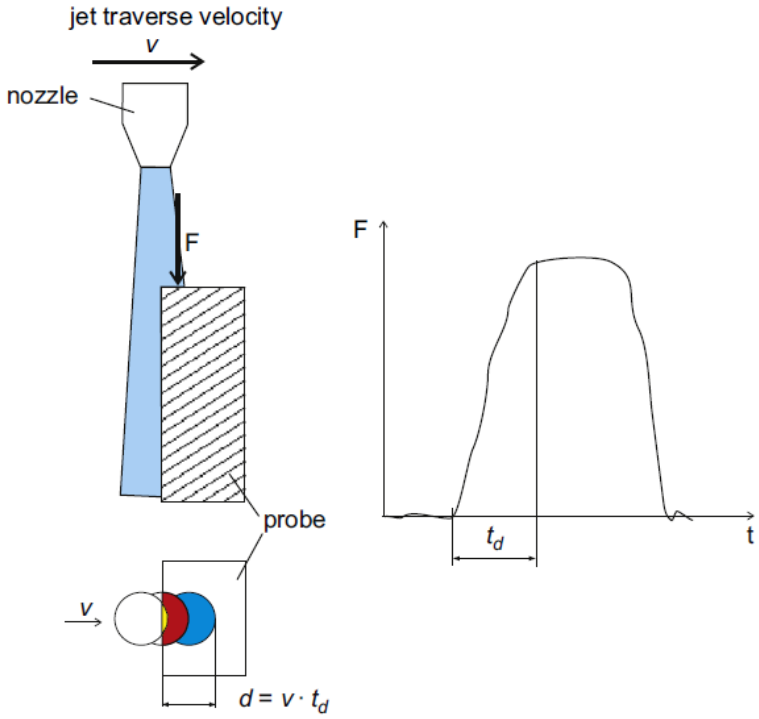

Figure 20: The principle of measuring jet diameter by measuring impact force [17].

The important part of measurement process is determining the correct start and end of time interval of the jet passing over the edge. The logical thing would be to look for the significant change in gradient of the curvature. But by doing so, the result can be overestimated. This is because the water droplets, which move around the core of the jet, produce the rise in the measured force. To eliminate this, a method was developed which first cuts off the influence of droplets and also automates the diameter measurement process. This is done by dividing the signal on three parts and fitting a line over each part. The three parts are shown in Figure 21 and are the following:

- Part 1: force is zero, the jet is approaching the probe
- Part 2: force is rising, the jet is passing over the edge of the probe
- Part 3: force has stabilized; the whole jet is on the probe.

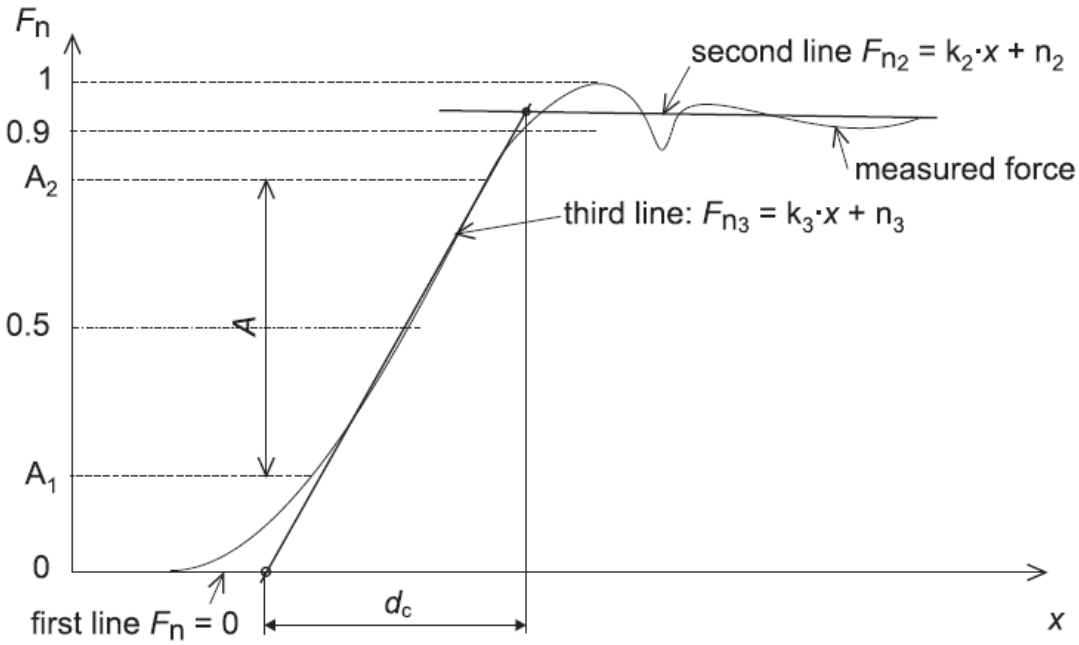

Figure 21: The three lines method [17].

This method does not need to use an additional laboratory to get the measurements, and the device is robust and resistant to moisture and residual abrasive effects are the mains advantages of load cell method.

However, the major difficulty in using this method for measuring diameter is the wear of the probe by the abrasive erosion. AWJ can machine almost any material as long as its hardness is lower than the hardness of the used abrasive. That is why the probe has to be made of a material which is as hard as possible. On the other hand it must not be too brittle as the passing of the jet can cause the crumbling of the edge of the probe.

4 Experimental setup

In this work, we used a digital camera to take photos of a high-speed water jet in the visible spectrum. To get the maximal quality of the photos, several modifications in the work ambient have been done, and several additional tools had to be created, and are explained below.

The phenomenological analysis of the water jet has been done combining visual observations with digital manipulation of the photography. We were modifying process parameters such as the diameter of the water nozzle, the water pressure and water temperature.

The measurement system used to perform the experiments is presented in the block diagram in Figure 22.

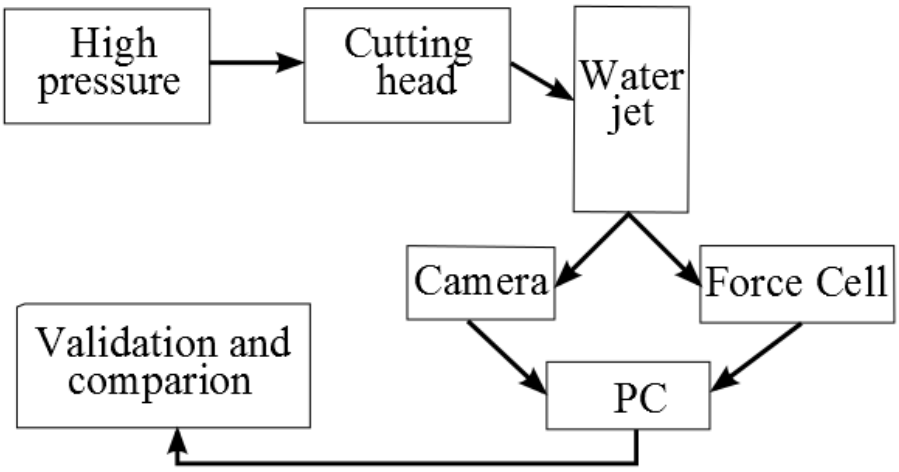

Figure 22: Block diagram of the measurement system for jet measurements.

In order to acquire digital images of the jet some additional installations have been set in the working area, as it can be observed in Figure 23.

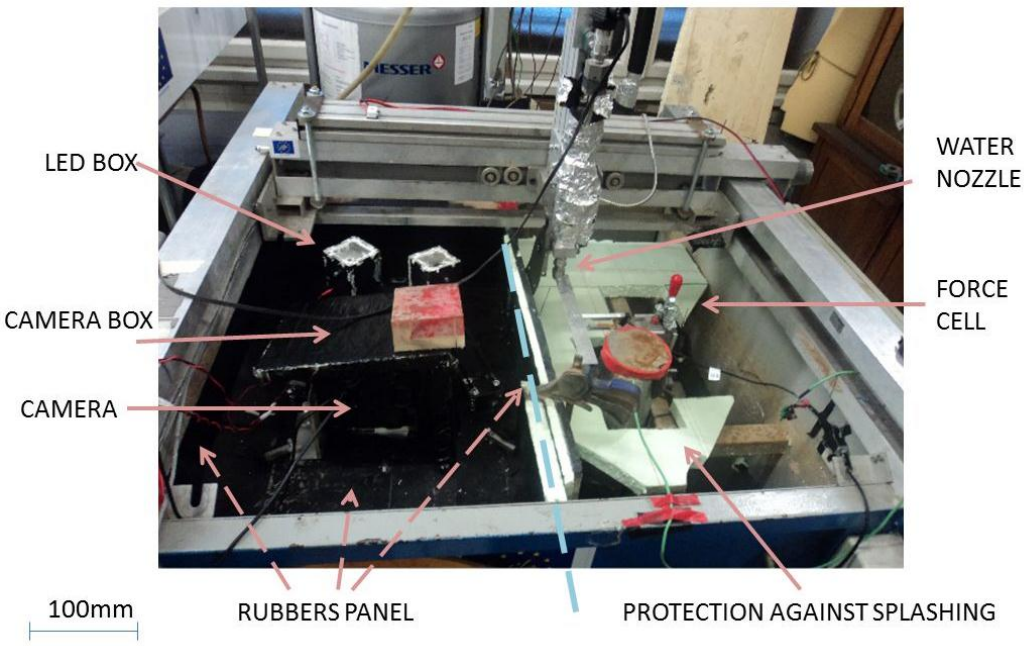

Figure 23: Experimental setup of the working area.

The imaging method shown on the left is composed of photographic equipment with a lighting system and a digital camera. Components were protected against water. In order to minimize the reflection of the light some rubbers were used. Positioning of lights and camera was achieved with a mechanical system able to get the focus of the light and the camera in the water jet.

On the right side the force method is composed of, a load cell to measure force.

4.1 Photographic equipment

To carry out this experiment in the IJ machining, in addition to the camera several additional tools were necessary to adapt in the system.

Camera

For photo capture the reflex camera Canon EOS 30D made in Japan presented in Figure 24 has been used.

Figure 24: Camera Canon EOS 30D.

This camera has a resolution of 8.2 Megapixel. It can take up to 3 frames per second, 14 frames burst performance and has 0.2 second start up time. The focal-plane shutter is electronically controlled at all speed, ranging from 1 / 8000s^{-1} until 5ms per 30 sec. The sensor, of a size of 22.5 mm x 15 mm, allows maximum resolution of 2336 x 3504 pixels [23], [18].

Platform illumination equipment and camera and the camera holder

As is shown in Figure 25, an aluminum platform was made to set the digital camera and the LED. The digital camera is arranged on the back of the platform, in the center of the symmetric of the source lighting. The LED lights are on the both sides in front of the digital camera.

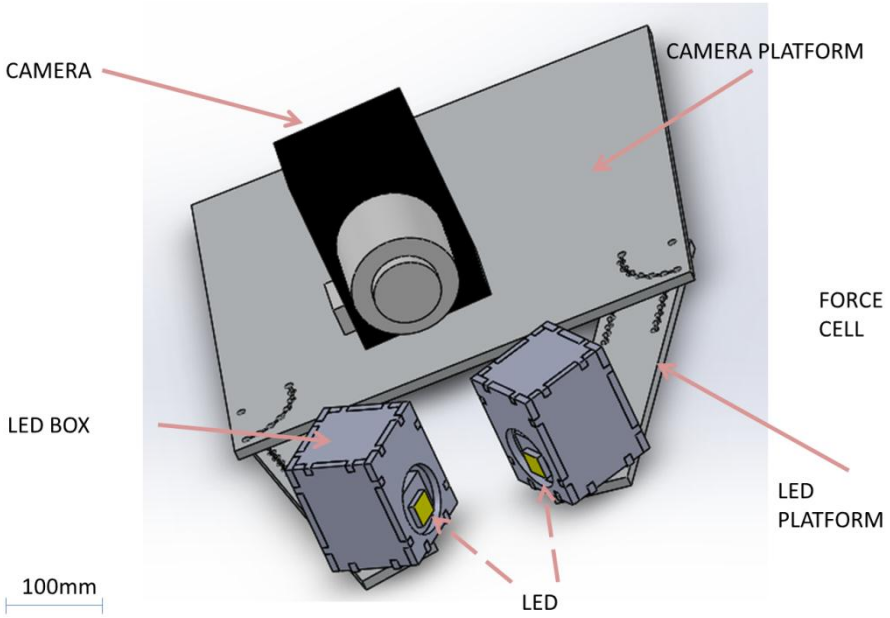

Figure 25: Design of the camera and LED lights platform.

The platform was created in several steps, which was made with the AWJ machining. Firstly, the geometry design was made by SolidWorks program, as is shown in figure 28. After this, to design and control of the AWJ, Omax Layaut and Omax Make respectively were used. Figure 26 shows the result of this process.

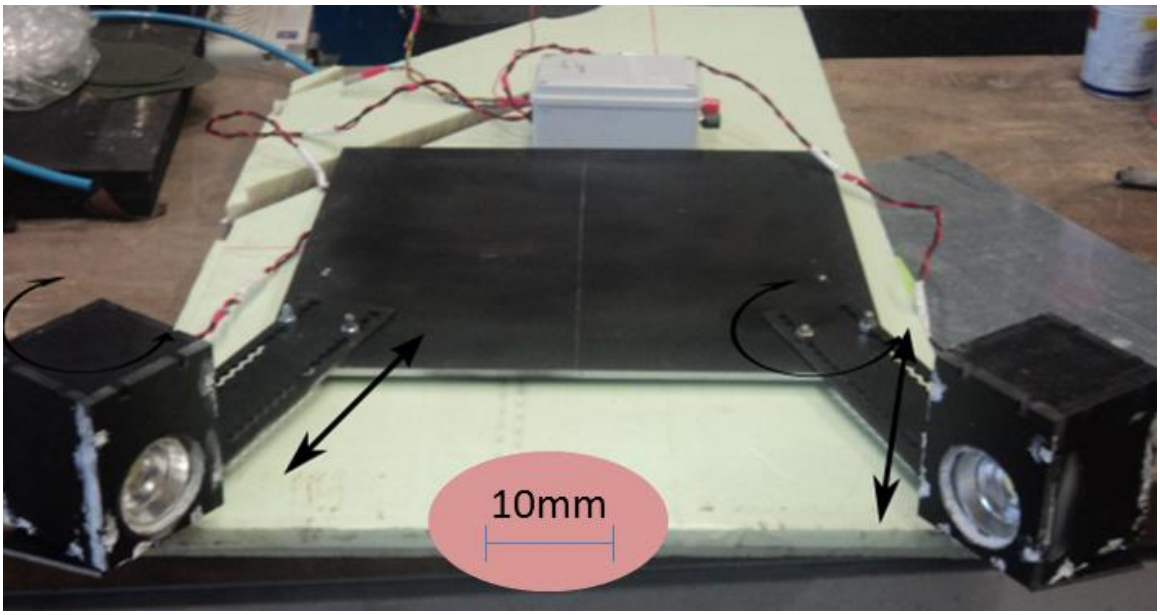

Figure 26: Platform illumination equipment and the camera holder.

The different movements of the components of the platform are indicated in Figure 26 using arrows. Due to these movements the most suitable position of the LED lights was determined.

Background and camera box

To prevent any backsplash of the water, to provide a good contrast and to minimize the reflection, a black rubber panel was used. The distribution of the rubbers is shown in Figure 27.

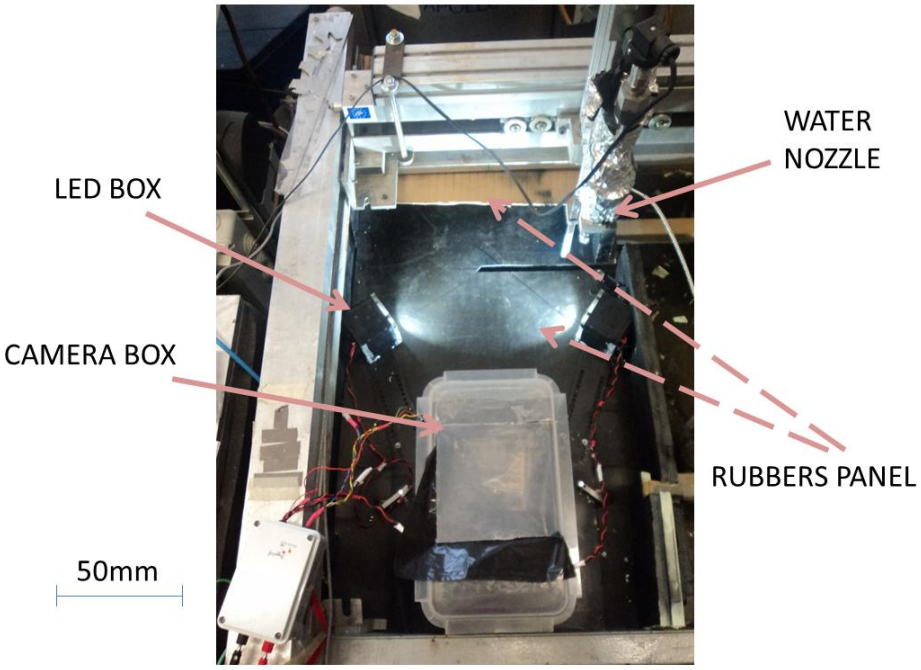

Figure 27: Protection against backsplash of the water.

The light reflection has to be reduced as much as possible to get an adequate sharpness in the photos. The first design of the box camera can be seen in the figure 31. Due to the final position of the led lights and of the camera we were not able to use it. The final design is presented in Figure 28.

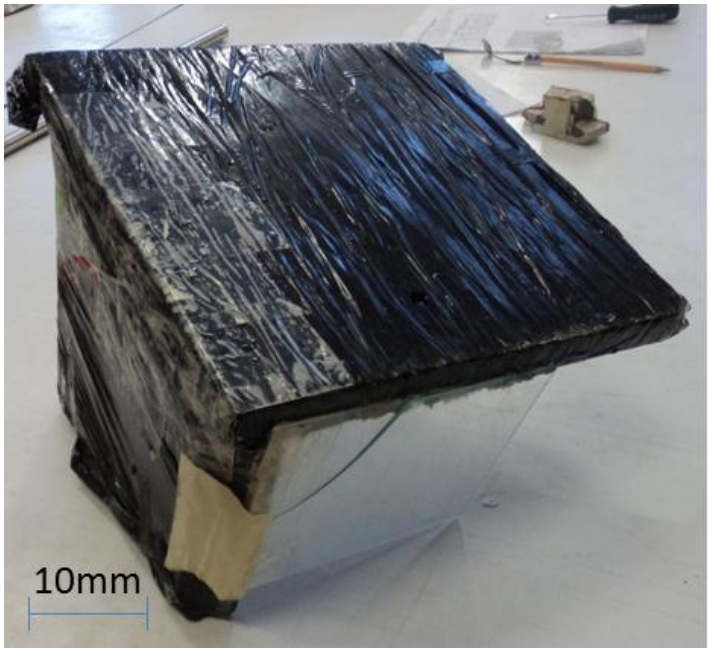

Figure 28: Plastic water protective box for the camera.

4.2 Measurement system

To carry out this research we used the Ice Jet prototype machine. In the work space we conducted two different researches simultaneously. Figure 29 shows the layout of the measurement equipment for both researches.

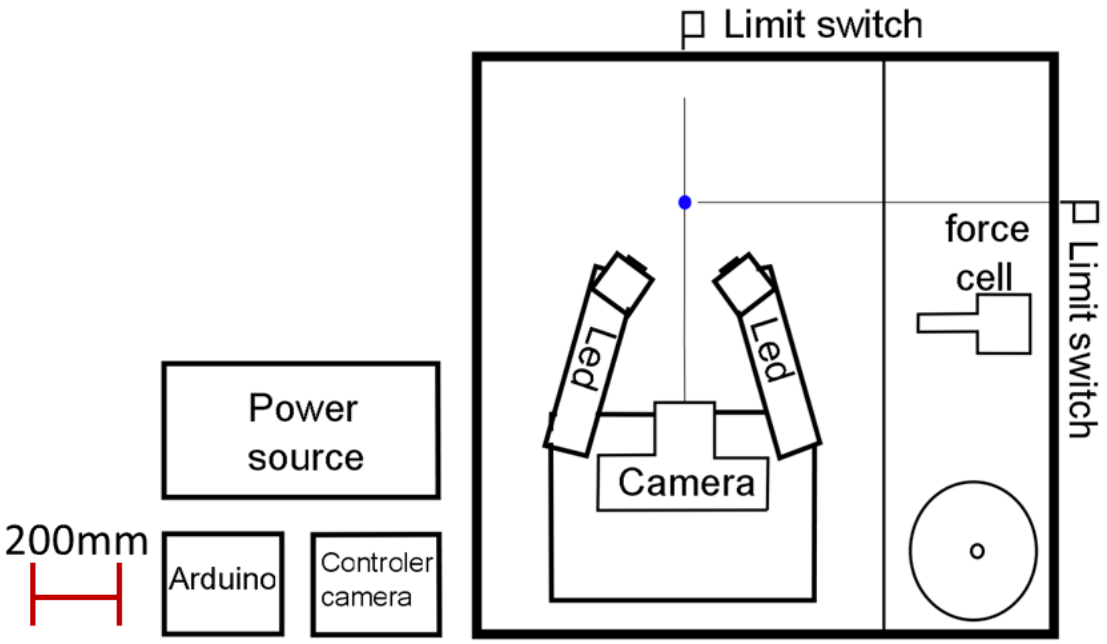

Figure 29: Schematic depiction of the test site for acquisition of the jet pictures and force data.

These researches aim to measure the diameter of the water jet. To get the photos with a properly quality, it is necessary to setup the lighting equipment. The load cell method, which has already been verified, was used as reference for the verification of the imaging method.

4.3 Illumination equipment

Putting this research into practice, involved several innovations to facilitate and improve the technology that was designed at University of Ljubljana [27]. This was necessary with the aim to get pictures of a better quality and consequently more accurate analysis results.

One of these improvements was the design and development of the illumination equipment. In order to achieve short shutter times and homogenous illumination of the measured area, a couple of high power LED was used. To get the total control of the LED a microcontroller was used.

One of the main reasons to use this kind of light is the size of the component. Led light is much more compact than conventional light, because the volume of the LED is around 0.2 dm^3 and the volume of the conventional light is approximately 8 dm^3. Components of the illumination equipment can be observed in Figure 30.

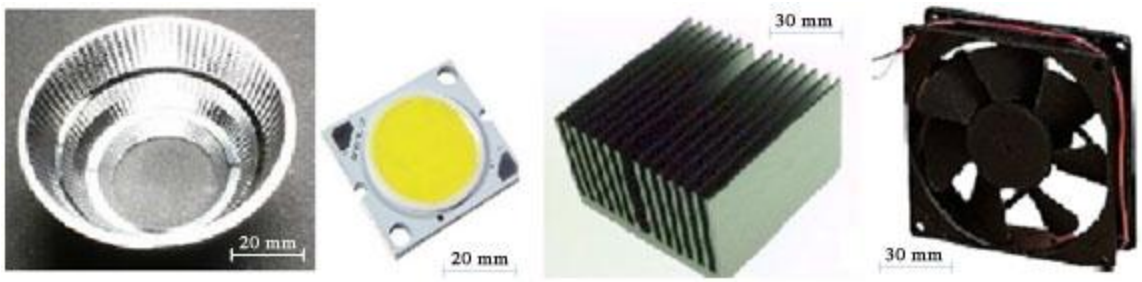

Figure 30: The reflector, LED, fan and heat-sink are components of the illumination equipment. LED light.

This huge difference in the size is quite important, if we want to design a prototype measuring device.

To achieve the proper illumination of the jet using two high power LED diodes, with 10.5 W each was a lighting system, using two high power LED diodes, with 10.5 W each, was used as shown in figure 31.

Figure 31: One of two high power LED diodes used for illumination of the jet.

One of the most important terms used in general illumination is correlated color temperature (CCT). CCT relates to the color of light produced by a light source, and uses the Kelvin temperature measurement scale (SI unit of absolute temperature). The cool white or Day White with CCT 5600K was chosen as it is the best for a movie studio.

The brightness of the LED is 1100 lumen, which it is the total amount of visible light emitted by led source, this value is enough to lighten the water jet length.

4.3.1 Schematic of the equipment lighting

To control short shutter times and homogeneous illumination of the measured area, a regulation for driving high power LED was used. This monolithic switching regulator is able to deliver constant and variable current to high power led light. An additional low power Mosfet was added just in case that we want to work with logic gates to get blinking of the LED. In Figure 32 the schematic of the lighting equipment is shown.

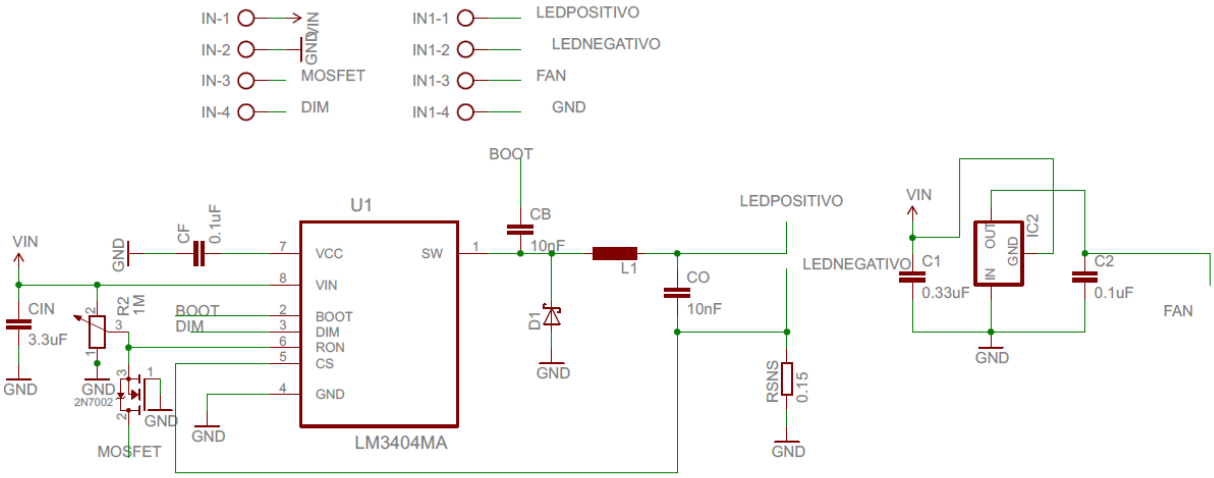

Figure 32: Electronic diagram LED light.

To get the values of the components for this schematic, the datasheet of the switching regulator [29] was used. To calculate the parameters was taken into account that the maximal possible value of the voltage is 21V and current of the LED is 1.2A.

To implement this schematic, which was designed in Eagle software, it was necessary to make a printed circuit board. To accomplish this ironing method was used. Due to the temperature variations in the workplace, because the temperature of the LED light it is not possible to know in advance, the fan schematic was added, just in case it was needed.

To design the printed circuit board (PCB) a software package CadSoft was used. This kind of software is a flexible and expandable application with schematic capture editor, PCB layout editor, auto-router and CAM. Eagle was selected, because the most of electronic components can be acquired for this program.

The main steps to carry out the printed circuit board single-side PCB can be seen in Figure 33.

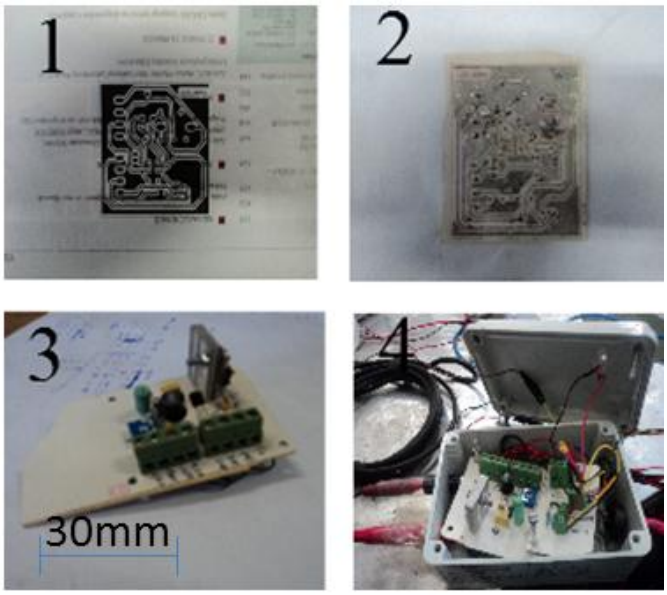

Figure 33: PCB layout (1), etching liquids (2), drilling (3), installation of components (4).

The PCB layout was shown in section 1 of Figure 33. The magazine paper was used, because that way it is easier to transfer the print to the copper plate. The quality of the print has the maximum contrast and blackness possible to get a good result.

To get the PCB to adhere to the copper, it is firstly necessary to flip out the paper and preheat the copper surface placing the iron on top. After 30 seconds the iron is removed and board is left to cool down.

When the board is cold enough to touch, the paper is submerged into water, and after trimming the excess parts. It is left to soak for one minute, or until paper softens. Then the paper has to be removed. If it has transferred correctly, it forms a very strong bond with the copper surface.

To get the section 2 (figure 33), to etching liquids the hydrochloric acid has been used. One has to be careful because it is concentrated enough to corrode any metal. In less than 10 minutes copper not covered by the ink is removed. Then the board has to be rinse with plenty of water. The last step to get the section 3 (Figure 33), drilling the component connection hole with 0.8 mm or 1mm of diameter. After drilling, to improve the appearance of the board and prevent the copper from oxidizing, the copper surface was created with a layer of tin.

The components were installed in their places and a box was used to protect the board against external agents such as water. The result of this process can be seen on figure 33.4.

4.4 Positioning, calibration and control of the illumination equipment

In order to get a good quality, the illumination equipment has to be positioned in the best possible way. The steps followed are further described. Firstly both LED lights have to be positioned symmetrically. The camera has to be set on their axis of symmetry. Then, the center of the focus of the light has to coincide with half of the length of the jet. After this, it is necessary to calculate the distance between led and jet, thus it is essential to know the typical viewing angle and finally, the distance between LED lights has to be long enough not to bother the field of view of the camera.

In Figure 34 the final position of the lighting equipment is shown.

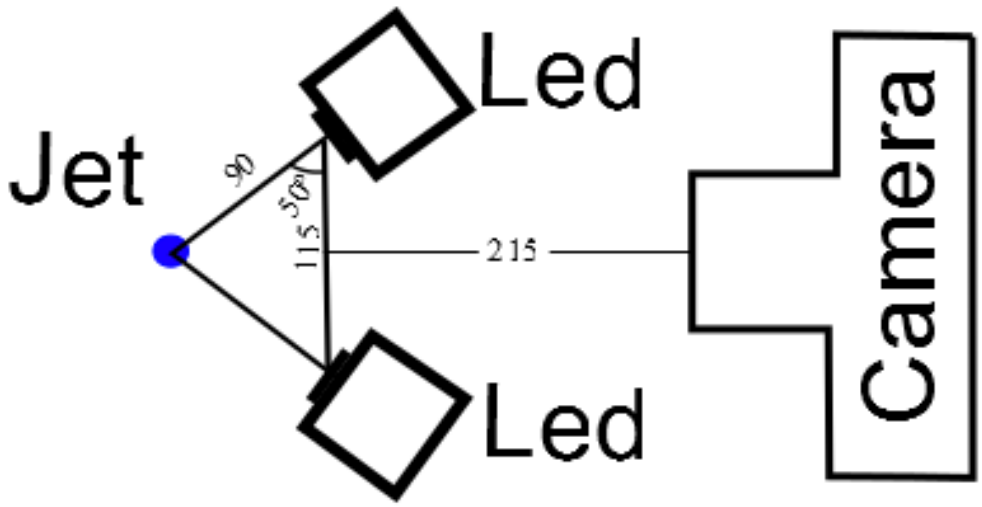

Figure 34: Positioning of the illumination equipment.

At the beginning the jet was located at the right side of the picture. Due to chromatic aberration of the lens, the violet colors on the right side of the jet were appeared. We could either get a better lens, but that could be expensive, or adjust the location of the jet from the right side to the center of the lens.

The difference between the starting arrangement and the corrected one, it can be seen in Figure 35.

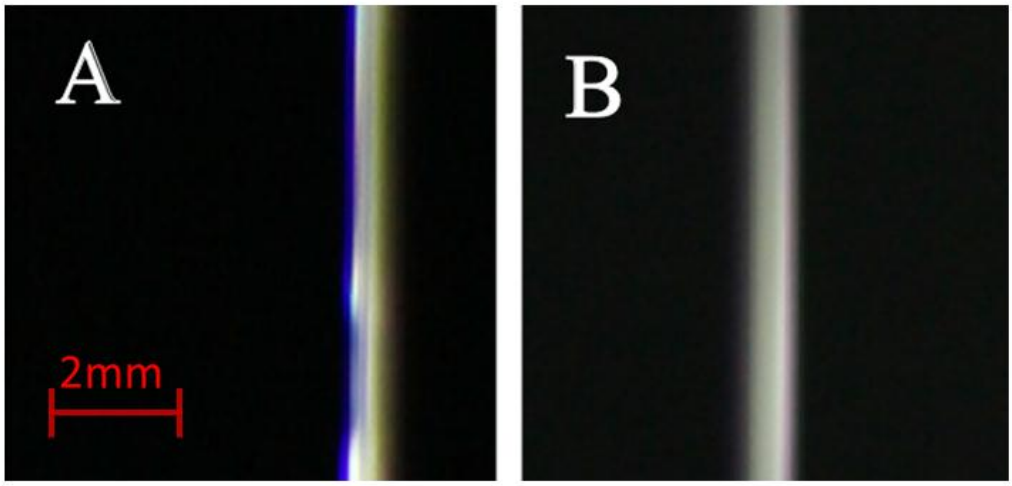

Figure 35: Differences between positioning of the jet in the right side (a), and the center (b) of the lens..

Several photos were taken looking through the viewfinder in order to find the proper distance between the jet and the camera. The distance depends on the focal range of the camera and the parameters fixed in the camera. To solve this, a parametric study has been done.

Image calibration

Image calibration was done using a ruler positioned along the center of the water nozzle from which it was possible to determine the pixel to millimeters ratio on each picture.

The ruler was also used to prevent the distortion of the photo and to have also the reference of the jet size, since it was easier to focus the camera. Figure 35 shows this system.

Figure 36: Image calibration system.

Due to the position of the ruler, as the two experiments take place at the same time and in the same place, the other tests are disturbed. To solve this trouble a few pictures of the rule were taken as a reference, in the same place where the water jet was later positioned, after this the ruler has been removed.

Images are analyzed in Matlab software package. The program codes can be seen in the attachment 10.1 and 10.2, at the end of this thesis. For the analysis of each image, the coordinates of the rectangle must be defined to determine the position of the reference levels and water jet as shown in Figure 36.

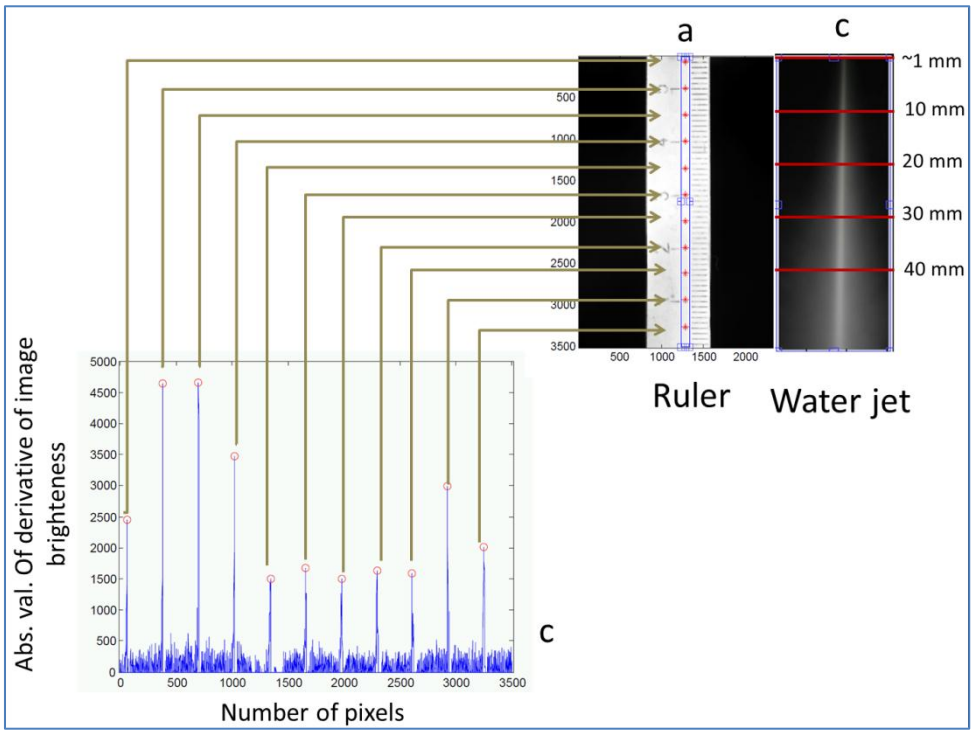

Figure 37: Calibration performed with the ruler. (a) It was placed along the center of the water nozzle. This allowed us to determine the pixel to millimeters ratio on each picture during the experiment (c).

The graph in Figure 37 shows the absolute value of derivative of brightness from y axis. Non-equal height is due to the non-uniform illumination of the ruler. Also markers on the ruler are not equally black. The calibration was performed once, because the distance between the jet and the camera was kept constant.

Remote control of the camera

One of the possible troubles the imaging method is due to some vibrations.

Consequently, power and high pressure can show up some vibrations in the head machining. This kind of problem is solved by fixing as much as possible all parts in the head machining.

Another possible vibration was caused when the shutter had been pushed. A remote control was installed to adjust this issue; the arduino controller was selected because it is a tool, which can be used to develop interactive objects, taking input from a shutter switch.

The program to control the number of the photos and the trigger and shutter can be found in the attachment 10.3 at the end of this thesis:

To make the PCB of the camera control, what is shown in figure 33, the same process than the schematic for the LED lights was done. In Figure 38 the schematic of the Photographic equipment is shown.

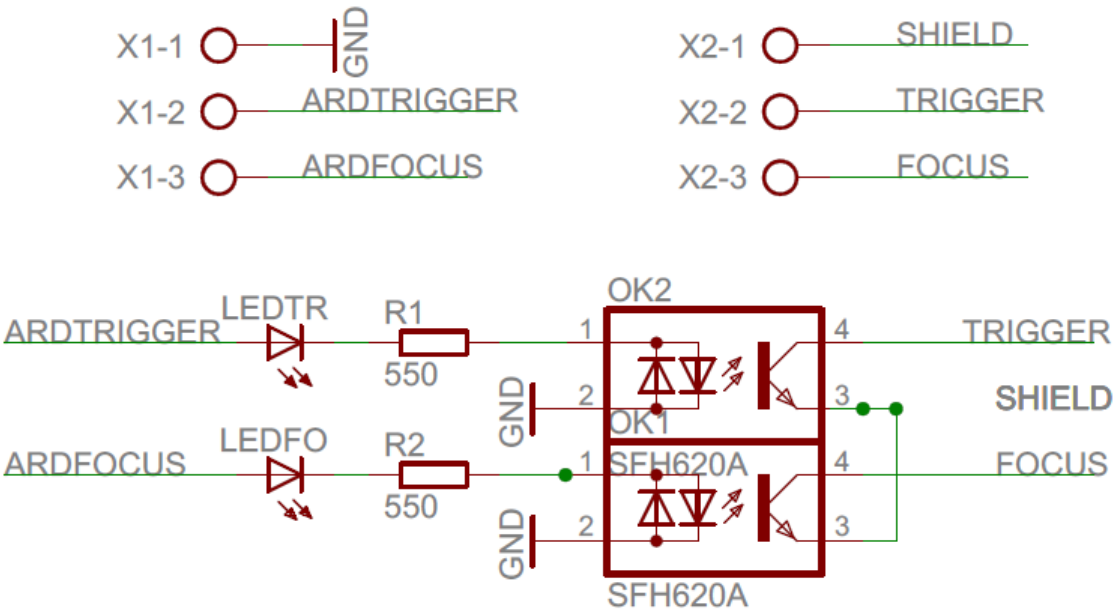

Figure 38: Electronic diagram camera control.

4.5 Parametric study

When setting up the digital camera parameters such as shutter speed, international organization standardization (ISO) and power of the LED were analyzed. Choosing the correct parameters for this type of photo analysis is difficult, because of the fog that is forming around the high-speed water jet, which is changing throughout the experiment.

As shown in Figure 39, if the power of the LED light is properly adjusted the fog issue can be solved.

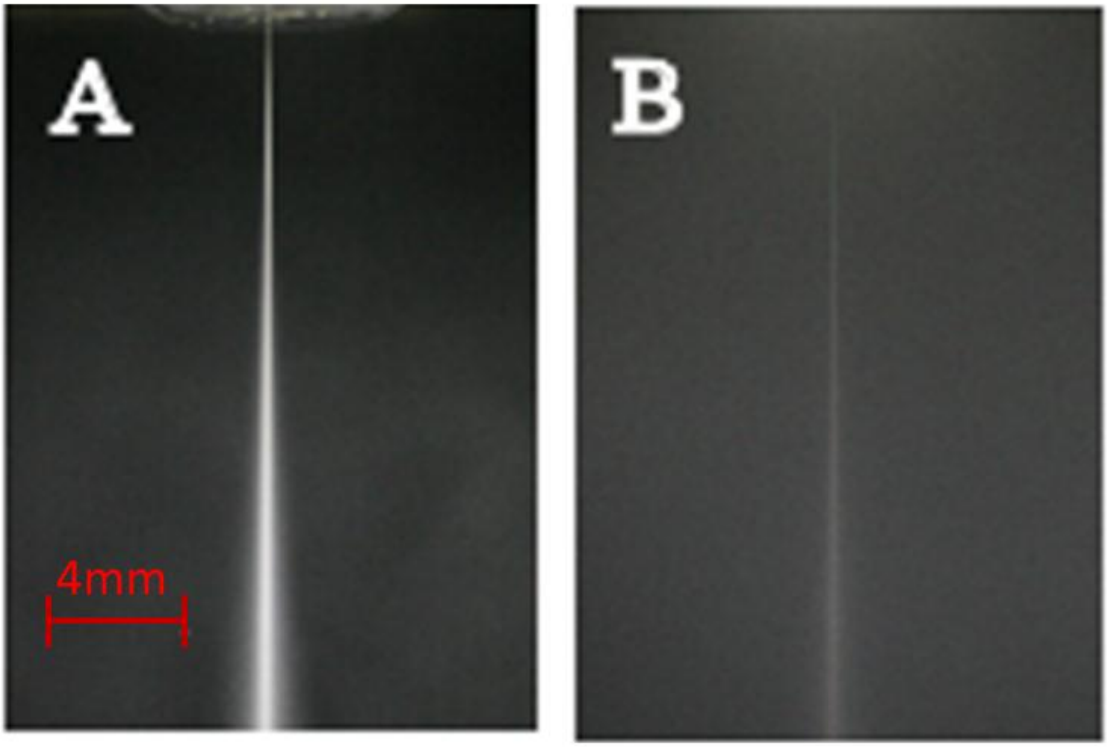

Figure 39: Pictures taken using different power of the light.

In Figure 39 the effect of the difference in the power of the LED lights can be seen. The Figure 39A is illuminated with a power of 10.71W and the Figure 39B has 6.41 W. The rest of parameters are presented inn Table 1.

Table 1: Parameters of the figure 39

P= 150MPa	Shutter speed=1250 s^{-1}
d_0= 0.2mm	EV=400 ISO
T= 23ºC	

The shutter speed shooter and exposure time are the effective length of time the camera shutter is open. The ISO values determine the sensitivity of the image sensor. The lower is its value, lower is the sensitivity of the camera light, and the finer the grain.

The ISO values ranges from 100 to 1600 to and the shutter speed values range from 30s to 1/8000 s. Keeping values of the power, the pressure, and room temperature constant, a study

of different values of the ISO and shutter speed has been done to select the best combination to get a good results.

In Figure 40, the value of the ISO was set 400 and the correct value of shutter speed was determined. When the shutter speed has a value of 5000 s^{-1}, the black background of the jet is more intensive, thus the balance between the black and white color on the picture is too black to be useful for analysis. On the other hand when the value is 1250 s^{-1}, this balance is in the opposite way. The value 2500 s^{-1} of the shutter speed has a regular balance, because of this was used.

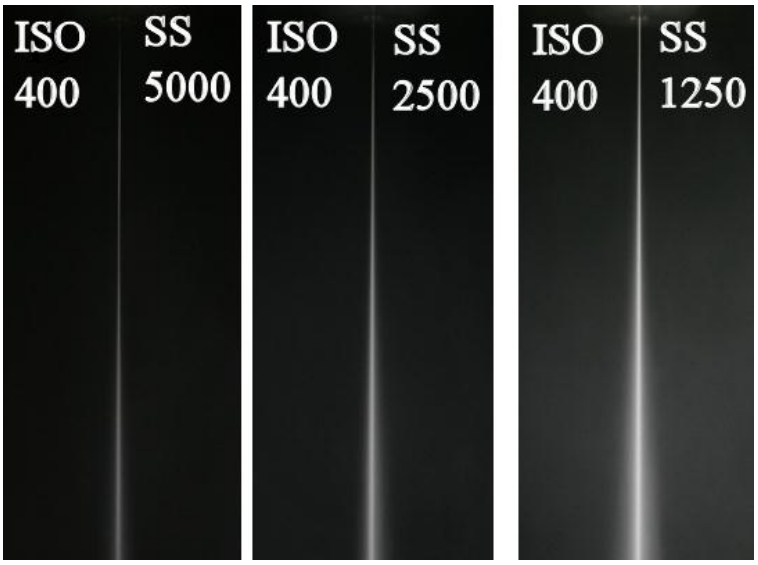

Figure 40: Modifying the shutter speed of the camera.

The rest of values from Figure 40 were:

Table 2: Parameters of the figure 40

P= 200MPa	P= 6.41W
d_0= 0.2mm	EV=400ISO
T= 23ºC	ISO= 400

In addition to analyzing the quality of the pictures to determine the value of ISO and the value of shutter speed, it has used the histogram of the camera to see the exposure level and the overall tone reproduction condition, there are two kind of histogram:

- Brightness histogram show the distribution of the image brightness level. The horizontal axis indicates the brightness level, where darker on the left and brighter on the right, while the vertical axis indicates how many pixeles exist for each brightness level.
- RGB histogram show the distribution of the brightness level for each primary color, which are red, blue and green.The horizontal axis indicates the brightness level of the color, where darker colors are on the left and brighter ones on the right, while the vertical axis indicates how many pixeles exist for each color brightness level.

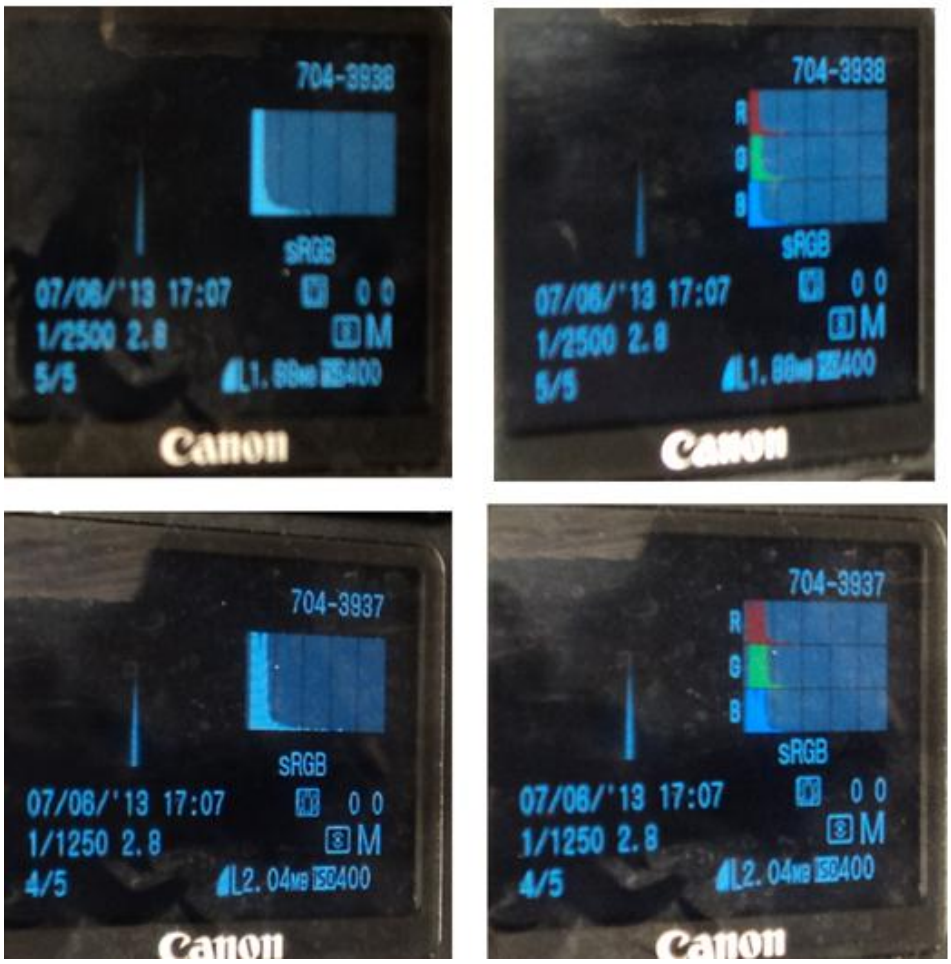

Figure 41: Histogram of the RGB (left) and Brightness (right).

Regarding the brightness histogram from Figure 41, there are too many pixels on the left, in the first level, which means that the photo are dark and also there are a few pixel closer to the right, it is means that the photo has a detail with highlight, which it is the jet.

When taking into account the RGB histogram from figure 40, too many pixels can be noticed on the left, the darker and less prominent the color.

4.5.1 Main parameters

In this research the influence of Temperature of the water nozzle (“T"), diameter of the water nozzle (“d_0”) and pressure (“P”) are searched.

The order followed to carry out all experiments was determined by the difficulty of modification of the parameters, being water nozzle temperature the value that requires more time and effort, while pressure is the easiest to be modified.

All of these parameters will have different values as follows:

- $T = [T_1, T_2, T_3]$ (ºC)
- $d_0 = [d_{01}, d_{02}]$ (m.m.)
- $P = [P_1, P_2, P_3]$ (MPa)

With these parameters the jet shape has been studied in 36 experiments, because of each experiment has been done with two different shutter speed values, 1250 s^{-1} and 2500 s^{-1}, and beside the number of the picture for each experiment was 28, the execution order shown in next table 3.

Table 3: Main parameters.

Number of experiment	Temperature	Diameter	Pressure
1			P1
2		d1	P2
3	T1		P3
4			P1
5		d2	P2
6			P3
7			P1
8		d1	P2
9	T2		P3
10			P1
11		d2	P2
12			P3
13			P1
14		d1	P2
15	T3		P3
16			P1
17		d2	P2
18			P3

For the experimental work ice jet machining was used, equipped with a high pressure intensifier pump and equipped with a heat transfer system. Three different pressures 150 MPa (P1), 200 MPa (P2) and 250 MPa (P3) have been used during the experiments in combination with two different diameters of the water nozzle 0.15 mm (d_{01}) and 0.20 mm (d_{02}) and in combination with three different water temperatures 23ºC (T1), 0ºC (T2) and -15ºC (T3).

To measure the temperatures 1.5 mm thick K-type thermocouples were connected to a USB-2416-4AO data acquisition card (DAQ) manufactured by Measurement computing (USA). Different positions of measuring system are shown in Figure 42.

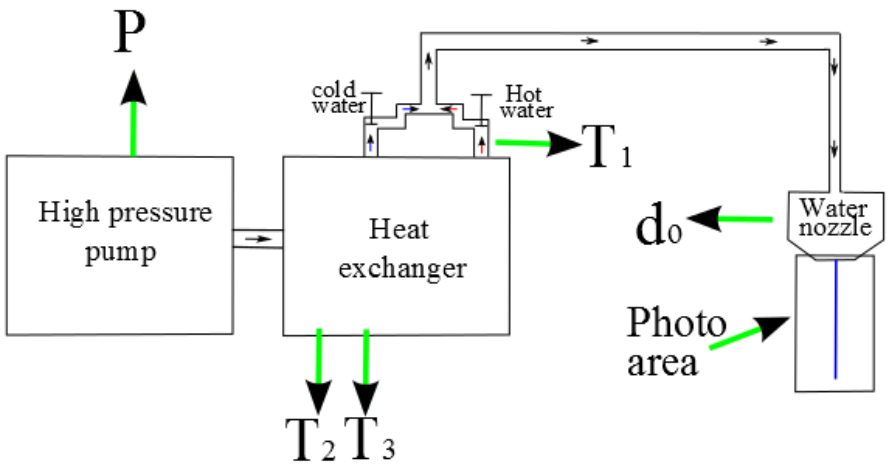

Figure 42: A schematic representation of experimental setup.

4.5.1.1 Water nozzle temperature

To get different temperatures of the water, the Ice jet generation, by super-cooling of pressure water, was used. To get temperatures lower than 0ºC the pressure of the water has to be according to the diagram of Figure 8. The heat exchanger was used, to produce a heat transfer from one medium to another until get desired temperature.

The cutting water is coming from a tank with antifreeze liquid, such as Glycol; this vessel has a high pressure valves, one for the cold water and the other for the hot water, the combination on both depends on the cutting temperature that we want to work with.

If cold temperature is wanted, it means that the cutting water is coming from the glycol tank, so the cold valve has to be open, and the hot water has to be closed. Respectively, if hot temperature is needed, the combination of the valves has to be in the opposite way. Both valves can be open at the same time, which means that the head machining is working with the mixt of temperature, but they cannot be closed simultaneously because the pressure that is coming from the pump does not have a way to go out.

Having a glycol tank permits to be able to work continuously with temperature values under 0ºC.The necessary time to achieve temperatures below 0ºC, with the heat exchanger is about 60min.

4.5.1.2 Water nozzle diameter

To modify the diameter of the water nozzle, one has just to replace this piece of the machining by other with different diameter.

The closing pressure of the water nozzle have to be 45 Newton meter, to do it properly the torque wrench was used, because the output of pressure water follows the model of conical

angle, which can be a modification if the water nozzle is closing with different value of moment. The water nozzle is show in Figure 43.

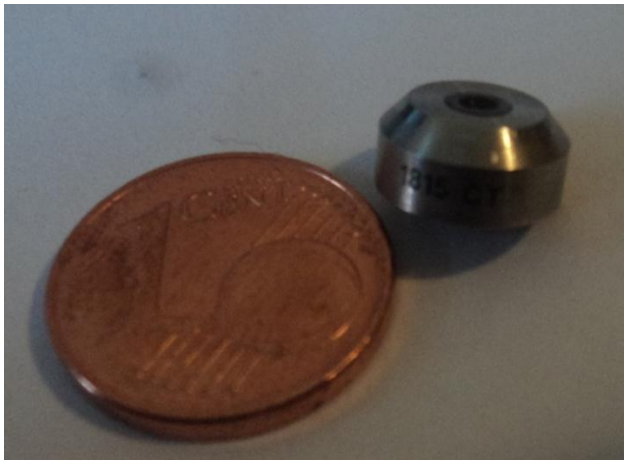

Figure 43: Water nozzle. Diameter is 0.15mm.

4.5.1.3 Pressure

To modify the pressure value the ice jet machining has a high pressure valve, figure 44, which it is very sensitive, but it is able to keep the pressure in a range of 1Mpa. As the temperature decreases, the pressure increase will be more difficult, because of the small ice particles formed in the valves.

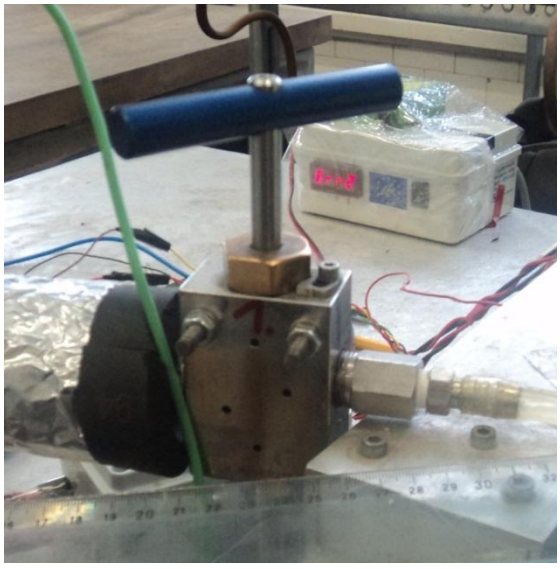

Figure 44: High pressure valve.

5 Analysis of the results

A comprehensive analysis of the results was made on the basis of images recorded with the camera. False color representation reveals the internal structure of jet. A Gaussian funtion was used to describe this structure.

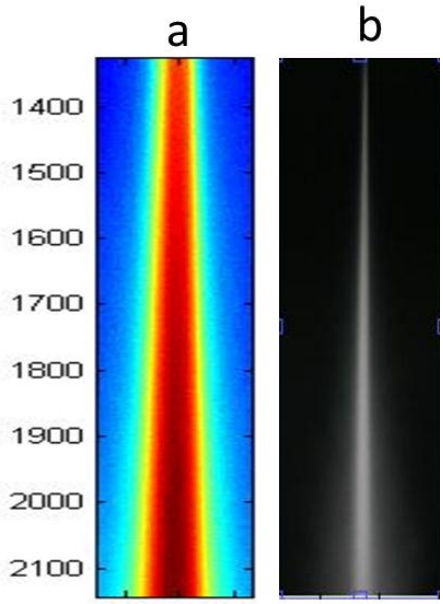

Figure 45: Different representation of internal structure of the jet.

In figure 45 the variation of velocity in the cross section of the jet can be discussed.

Velocity of the water is lower in the outer layers of the jet, while the one in the center of the jet is faster, due tu the friction forces between the jet and the surrounding air.

Opposite effect is due to the surface tension which pulls the jet together. Oscilations between both forces cause jet to slowly desintegrate, producing the droplets and surrounding fog. Due to the difference in speeds between the surrounding air and the high-speed water jet, the turbulent eddies form around the jet. Eddies grow bigger further along the jet. These eddies contribute significantly to the jet disintegration process.

Figure 46 shows how water surface tension decreases with temperature. This is because cohesive forces decrease as molecules vibrate at a higher frequency when temperature is increased.

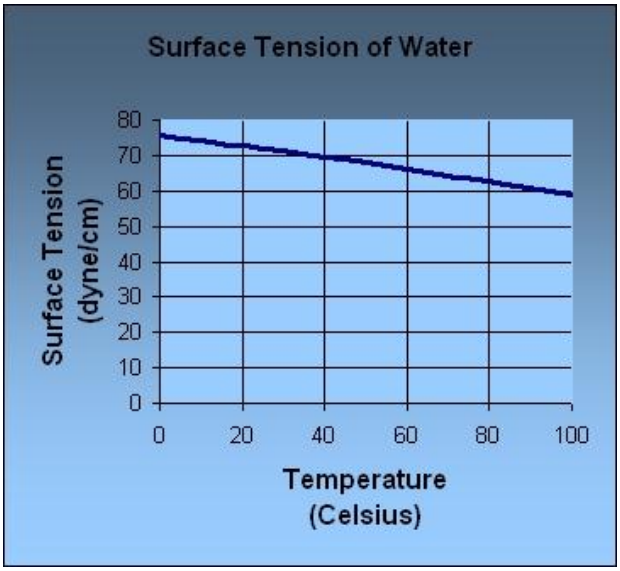

Figure 46: Variation of surface tension with temperature 0.

5.1 Model function selection

The brightness at each row of the jet image taken during the experiment was modeled by a Gaussian function.

Gaussian function is a continuous and defined by the equation (6.2)

$$f(x) = \frac{1}{\sigma\sqrt{2\pi}} e^{-\frac{(x-\mu)^2}{2\sigma^2}}. \qquad (6.2)$$

In the equation 6.2, the parameter μ is the mean or position of the center of the pear and σ is its standard deviation or the width of the shape.

The influence of these parameters on the shape of the Gaussian curve is shown in Figure 47.

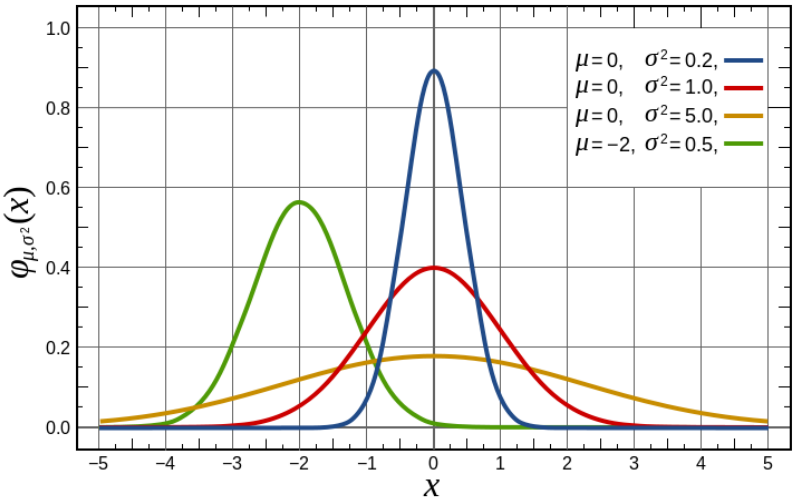

Figure 47: Plots for different parameters of Gauss function.

Figure 48 is an illustration of typical Gaussian curve obtained during experiments. The diagram shows the measured values of the brightness of the particular row of the image and the adapted values by Gaussian curve.

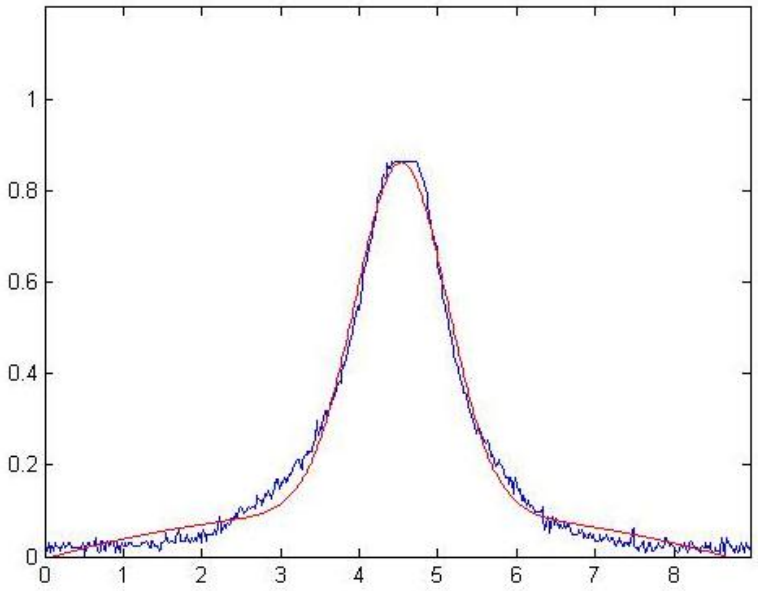

Figure 48: Diagram which shows the measured values of the imaging method (blue line) and adapted Gaussian curve (red line).

6 Results

In the Figure 49 the radial dependence of the image brightness at five different stand-off distances shown. The interval value between the measurements is 10 mm. The values presented in this figure are derived from the experiment number 15. This interval of measures was chosen to compare them with the force method measurements.

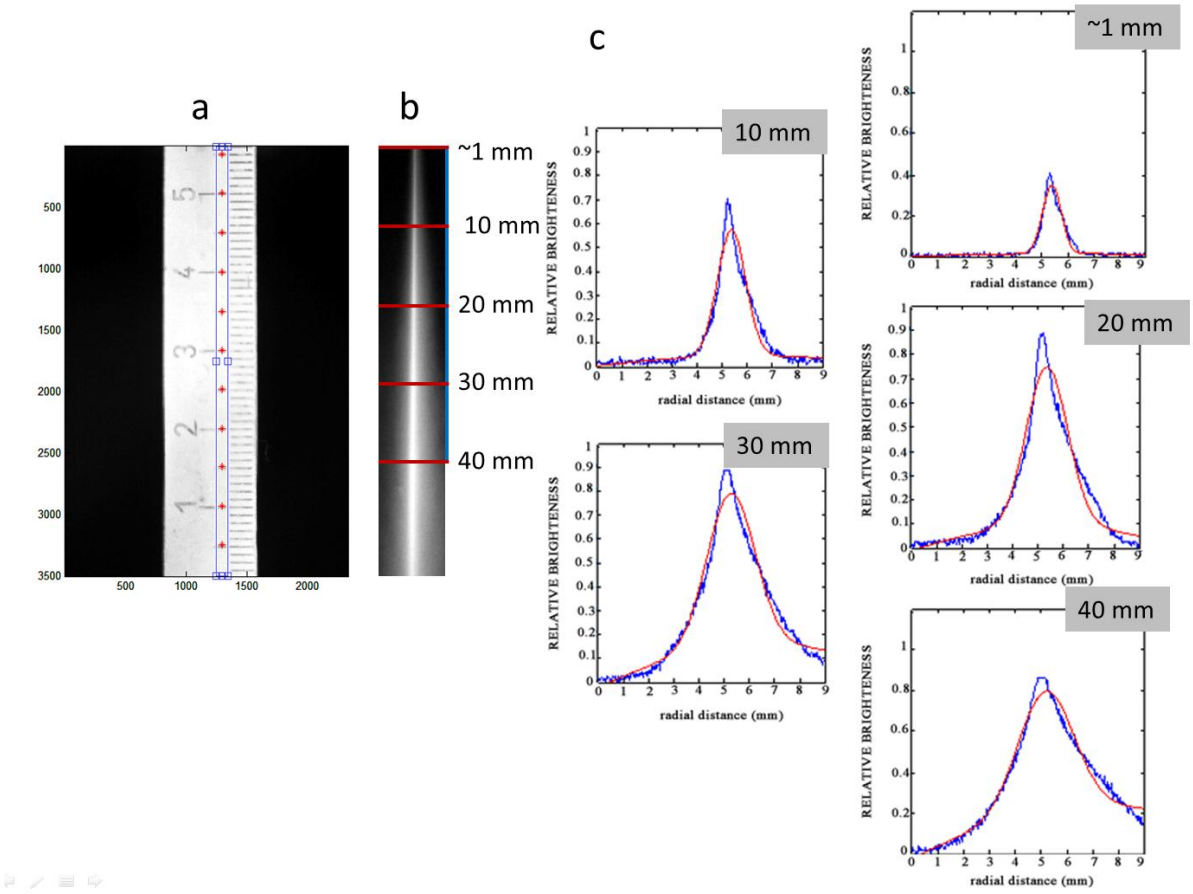

Figure 49: Illustration of typical relation between jet divergence and stand-off distance. Calibration ruler (a) and jet image (b).

Figure 49 shows the increase in the jet width. It means that diameter depends on the distance from nozzle.

Table 4: Standard deviation values of the experiment 15.

Stand off	Unit (mm)	Average of STD	Standard deviation	STD error	Error percentage (%)
1	~1	0.304348	0.040821	0.018256	6
2	10	0.460482	0.072847	0.032578	7
3	20	0.675812	0.074494	0.033315	5
4	30	0.852596	0.100819	0.045087	5
5	40	0.941515	0.123728	0.055333	6

Jet shape widens its value according to the distance from nozzle, while the error percentage in the measurement stays almost constant.

The measurement of the force method is defined in 5 different levels, the distance between levels is 10mm, and the repetitions of the experiment are done 10 times per level.

One repetition of 10 ones possible for experiment 15 is shown in Figure 50.

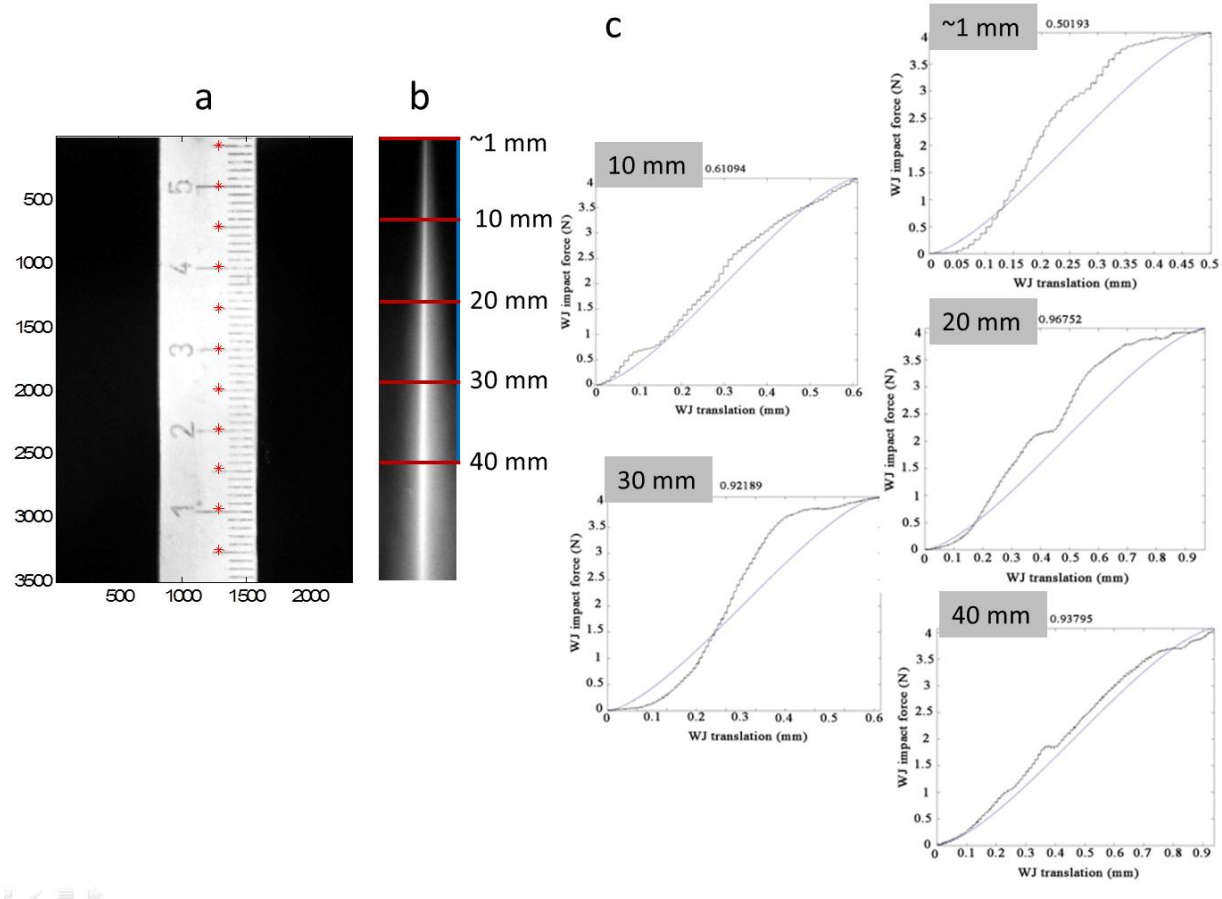

Figure 50: Illustration of a typical relation between force measurements and stand off distance.

Figure 50 shows as jet diameter, which was calculated with the force cell, changes along with the length of the water jet.

Table 5: Force measurements values of the experiment 15.

Stand off	Unit (mm)	diameter (mm)
1	~1	0.50193
2	10	0.61094
3	20	0.96752
4	30	0.92189
5	40	0.93795

6.1 Verification of the method

The main point of this master thesis is the verification of the imaging method. Validation and composition between jet shape measurement by imaging method and jet pressure measurement were done simultaneously. Both methods have been studied with the same conditions of water temperature, water nozzle diameter and pressure.

To be able to compare the two methods, it is necessary to find a factor which binds the two solutions, due to the fact that the analysis result of the measurements is obtained in a different manner. The force method permits to achieve directly the value of the diameter of the water jet; while the imagining method provides with the standard deviation.

The common factor at issue is:

$$f = \frac{d_f}{std} \qquad (7.1.1.a)$$

Where d_f is the jet diameter obtained through the power method and

Sdt is the standard deviation obtained with the imagining method.

From one point of view, the power method allows the determination of the jet diameter values in a range of 10 mm of distance between the levels. On the other side, the values of the standard deviation can be obtained through the imagining method along the whole length of the water jet.

Consequently, the values of the standard deviation will be obtained through the use of the imagining method in the intervals of 10 mm of distance between the levels.

Quality of the photo:

The image capture has been done with two different shutter speeds. The value of shutter speed could be 1250 s^{-1} and 2500 s^{-1}.

In the table 4, calculation of Calibration factor for both shutter speed can be found and in the attachment 10.4 at the end of this thesis has been added the process of calculation.

Table 6: Calibration factor for both shutter speed.

Averages		
Stand off	**f(SS1250)**	**f(SS2500)**
1	0.053416	0.056891
2	0.083173	0.080304
3	0.101853	0.096458
4	0.124501	0.119541
5	0.129077	0.116567

Figure 51 provide the results regarding the average coefficient of the standard deviations for each value of shutter speed. It can be observed that our analysis results do not depend on working shutter speed, thus we choose one of them to carry out the analysis.

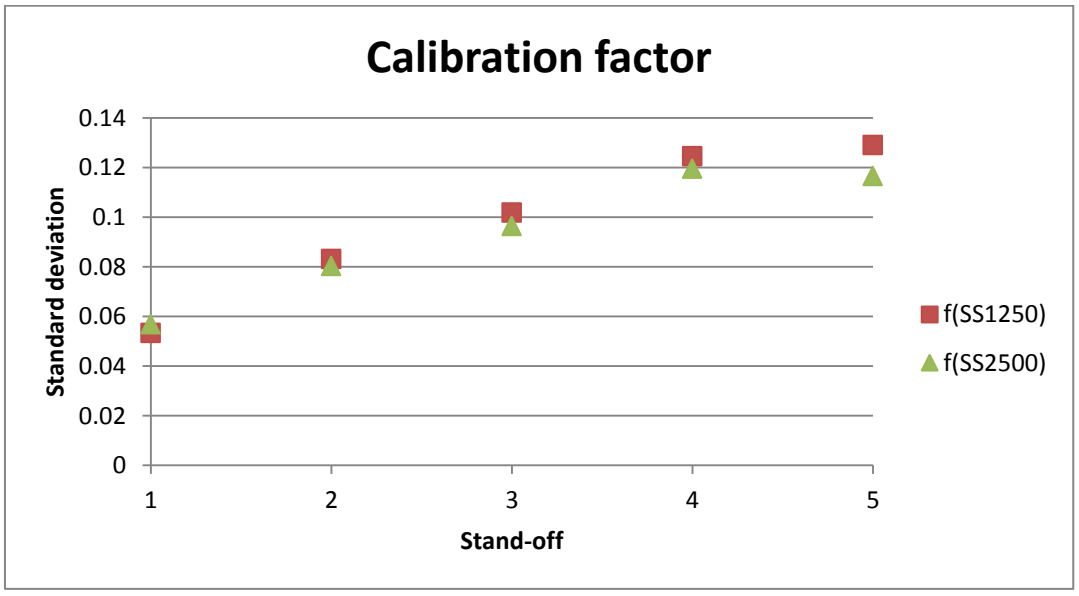

Figure 51: Calibration factor for both Shutter speed, where the y axis is the standard deviation value and the X axis is the stand off.

To know how shutter speed influence on the results of the standard deviation, another group of photos was done with different value of shutter speed. The new value is 5000 s^{-1}

In Figure 52, a photo per Shutter speed is shown.

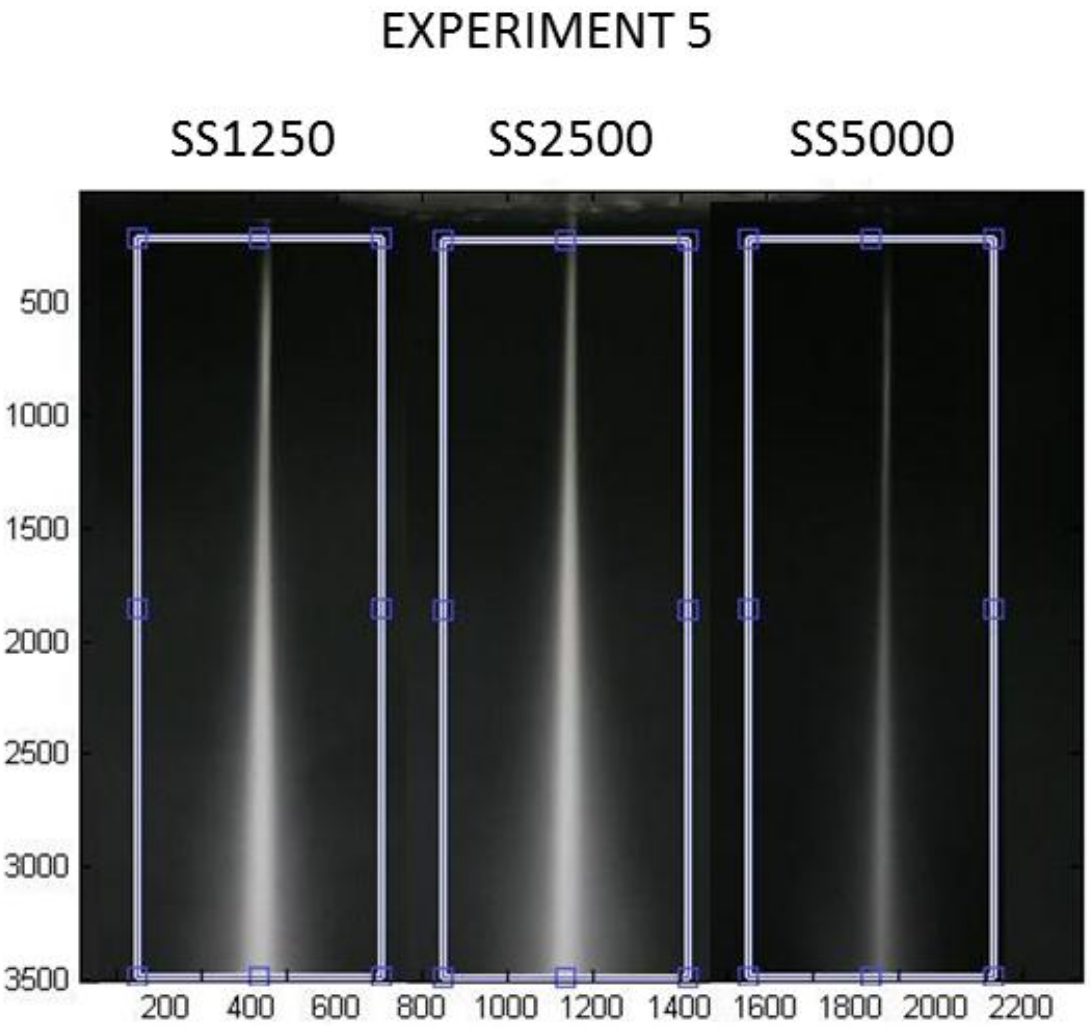

Figure 52: experiment 8, shutter speed 5000 s^{-1}.

In the table 7 different values of standard deviation for the experiment 5 can be seen.

Table 7: Calibration factor for each Sutter speed of the experiment 5.

Experiment 5			
Stand-off	**f1250**	**f2500**	**f5000**
1	0.028867	0.015709	0.022526
2	0.070496	0.048728	0.023654
3	0.076	0.083874	0.041649
4	0.100451	0.10687	0.068959
5	0.142972	0.242108	0.052303

Figure 53 provide the results regarding the coefficient of the standard deviations obtained for the experiment 5.

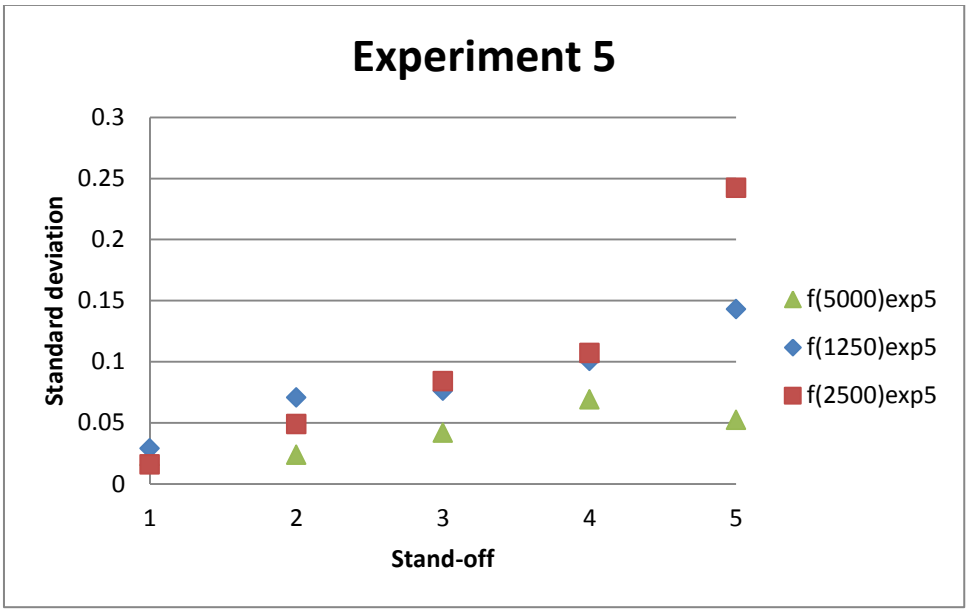

Figure 53: Calibration factor for each Shutter speed of the experiment 5, where the y axis is the standard deviation value and the X axis is the stand off.

In figure 54 are provided the results regarding the coefficient of the standard deviations obtained for the experiment 5, although the brightness decreases with the increase of the shutter speed, as it is shown in Figure 53. Observing the result it can be seen, how the values of standard deviation coefficient for each stand-off are similar until the stand off 4 because of the fog, but there is a small distance between them in the column number 5.

Correlation between two methods

The average value defined for each of the force measurement levels have been analyzed

Figure 54 and 55 points out the correlation between the average of the force and the calibration factor. The asterisks of the figure represent the different values of stand-off of each experiment

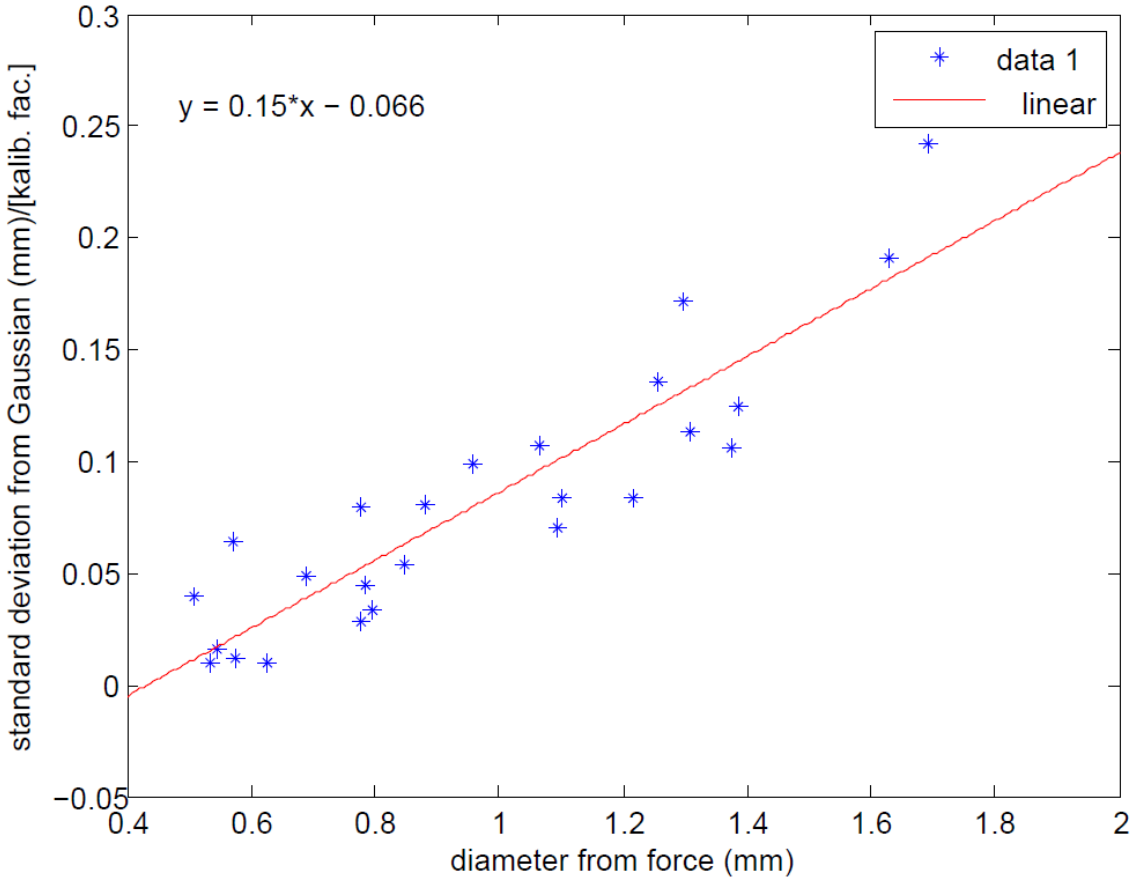

Figure 54: Calibration curve for shutter speed 1250 s^{-1} and the average of the force.

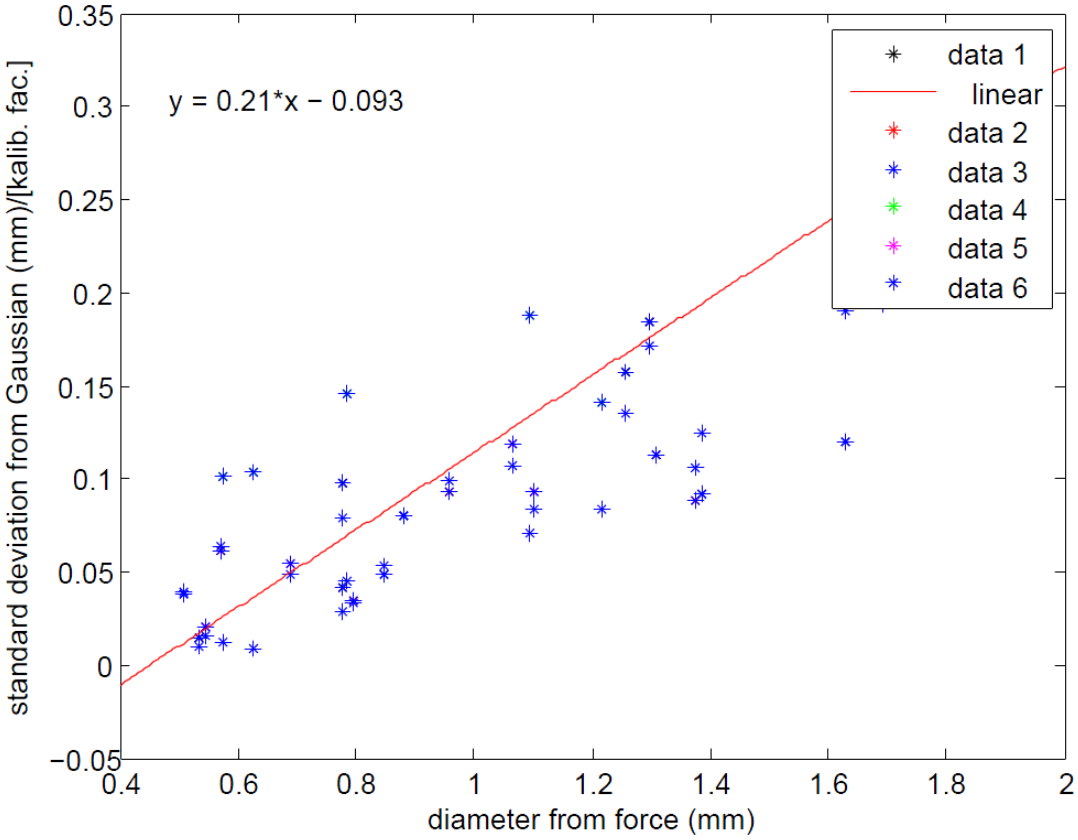

Figure 55: Calibration curve for shutter speed 2500 s^{-1} and the average of the force.

It is clear and also expected, that diameter based on the average coefficient of the standard deviations is smaller than diameter based on force measurement.

Dispersion of the asterisks appears because of the possible sources of measurement uncertainty; in further researches the results of the presented study have to be critically studied in order to find a way to identify and eliminate them.

6.2 Validation

To validate this Calibration curve several examples with different force measurement were done.

Figure 56 shows the result of correlation between averages of force measures of the experiment 5.

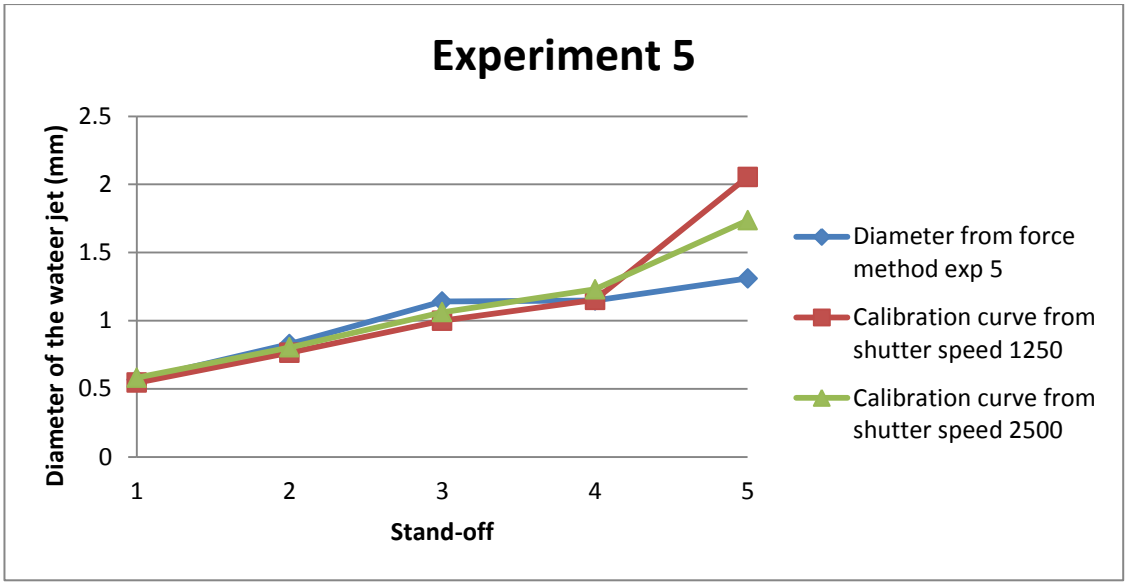

Figure 56: Calibration curve and average force measures of the experiment 5.

Table 8: Calibration curve and average force measures of the experiment 5.

stand-off	Standard desviation from exp5 with shutter speed 1250s^{-1}	Standard desviation from exp5 with shutter speed 2500s^{-1}	Diameter from force method exp 5 (mm)	Calibration curve from shutter speed 1250(mm)	Calibration curve from shutter speed 2500 (mm)
1	0.015709	0.021129	**0.565584**	**0.544724**	**0.580859**
2	0.048728	0.054419	**0.827416**	**0.764852**	**0.802793**
3	0.083874	0.093165	**1.139987**	**0.999158**	**1.061097**
4	0.10687	0.118478	**1.147889**	**1.152465**	**1.229853**
5	0.242108	0.194378	**1.309647**	**2.054053**	**1.735852**

Figure 57 and table 9 show the result of correlation between average of force measures of the experiment 13.

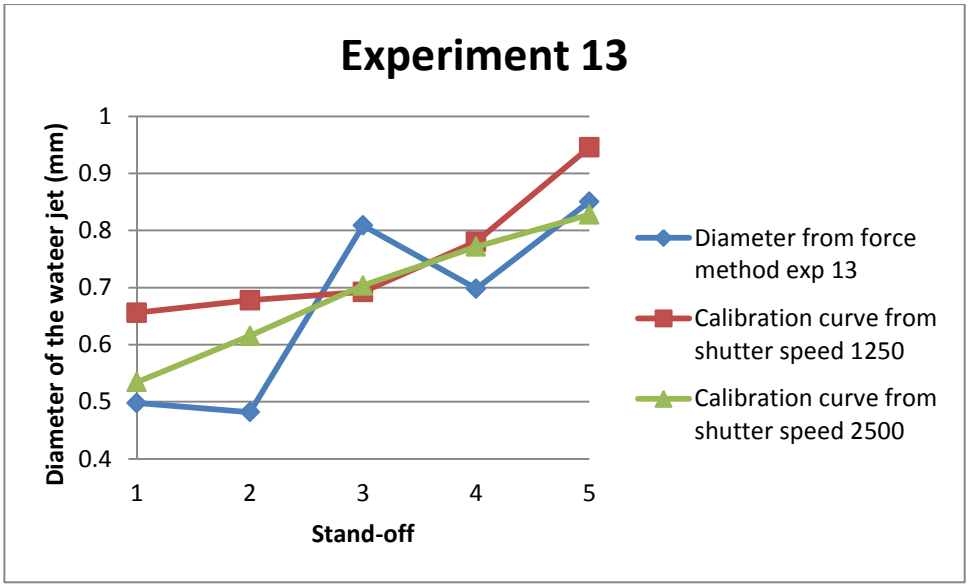

Figure 57: Calibration curve and average force measures of the experiment 13.

Table 9: Calibration curve and average force measures of the experiment 13

stand-off	Standard desviation from exp13 with shutter speed 1250s^{-1}	Standard desviation from exp13 with shutter speed 2500 s^{-1}	Diameter from force method exp 13 (mm)	Calibration curve from shutter speed 1250s (mm)	Calibration curve from shutter speed 2500s (mm)
1	0.044767	0.019263	**0.565584**	**0.656033602**	**0.534584**
2	0.049333	0.036301	**0.827416**	**0.677777805**	**0.615718**
3	0.052397	0.05474	**1.139987**	**0.692368582**	**0.703524**
4	0.070895	0.069056	**1.147889**	**0.780451425**	**0.771697**
5	0.105553	0.080858	**1.309647**	**0.945488601**	**0.827895**

Both Figure 55 and 56 show that there is a linear correlation between the calibration curves and the diameter of the water jet.

7 Discussion of the method

According to the results of this report, we can state that this method is enough to carry out further research. Besides being able to get better results using the beta function instead of Gaussian function, it can also be performed by other types of image shooting.

7.1 Stroboscopic effect

The stroboscopic effect is a visual phenomenon caused by aliasing that occurs when continuous motion is represented by a series of short samples and the moving object is in lineal motion at a rate close to the sampling rate.

To get a good result with the stroboscopic effect, both frequency of the blinking LED and the water speed jet have to be synchronized.

To carry out this experiment the water speed jet has to be obtained, it is necessary to make a program with Arduino, where the frequency of blinking LED light can be increased or decreased.

After finding blinking frequency, the water jet can be seen by one's eyes as if it would be immobile. Knowing the frequency of blinking of the LED light, the stroboscopic effect can be used, thus the shutter speed and firing frequency can be calculated. This way, better quality of the picture can be achieved, and accordingly better analysis result can be obtained.

7.2 Industrialization of the method

Other possible research on this method would supposed to make of a platform composed of a lighting system and camera. Thus the imaging method can be used easily as a measuring instrument, regardless of the lighting effect (for example stroboscopic effect) that you want to give.

8 Conclusion

In this Master thesis the phenomenological analysis method of water jet diameter measurement has been explored. In this experimental method it was necessary to combine digital image acquisition and processing by digital manipulation of the photography.

To carry out the experiment with the Ice Jet (IJ) machining, it was necessary to adapt the working area with illumination equipment and photographic equipment. Simultaneously a set of measurements of WJ force has been made with the load cell for validation of the novel method. More than one thousand photos of the jet were acquired during experiments in which WJ process parameters such as pressure, water temperature and diameter of the water nozzle were changed.

According to the results of the image analysis, which was performed in the Matlab software package, we got to several conclusions. A linear relation has been found between the jet diameter and the width of radial dependence of image brightness (standard deviation). For the comparison the jet diameter has been obtained through the force method also.

Regarding the correlation between the diameter and the width of radial dependence of image brightness, it can be stated that it is possible to define the jet diameter using the imagining method.

To determine the correlation between WJ diameter measurements obtained by force and photographic method, results of presented study has to be critically studied in order to find a way to identify and eliminate the possible sources of measurement uncertainty.

Further, it can be claimed that the camera method is much faster than the force one. Moreover, the geometry all along the jet can be obtained through the camera method at once, where with the WJ diameter measurement by force method only the measurement at a specific distance from the water nozzle in each measurement.

The imagining method gives much more reasonable results in advance than the force method, and the only crucial factor is time.

9 Literatura

[1] Marko Jerman; State of the art report on Ice Jet Technology, Life.

[2] Version 2 ME, IIT Kharagpur. Module 9 (Non-conventional Machining)

[3] Marko Jerman, H. Orbanic, I Etxeberria; 2011 WJTA American Waterjet Conference.

[4] E. Geskin, L. Tismenetskiy, F. Li, "Development of Ice Jet Machining Technology", NJIT, *8th American Water Jet Conference*, 1995, pp. 671-680.

[5] P. Truchot, P. Mellinger, and R. Duchamp, "Development of a Cryogenic water jet technique for biomaterial processing applications", *6th American Water Jet Conference*, August 17-19, Houston, Texas, WJTA, Omnipress: paper 3-G, 1991, p.473-480.

[6] Marko Jerman and Henri Orbanić; Ice Jet Machining technology for the greener tomorrow

[7] M. Jerman, A.Lebar, M. Junkar; Measurement and modeling of the water jet shape.

[8] J. Folkes, Z. J. Li, "Inovative method of waterjet jet diameter measurement for process and quality control'', in: Proc. 20th International conference on Water Jetting, BHR Group, Graz, Austria, 2010, p. 329-498.

[9] S. Shimizu, t. Ishikawa, A. Saito, and G. Peng, ''Pulsation of abrasive wter-jet'' in *2009 American WJTA Conference and Expo*, August 18-19, 2009 Huston, Texas, paper 2-H.

[10] Manufacturing Engineering and Technology Fifth Edition –Serope Kalpakjian and Steven R. Sschmid (Prentice Hall),2006.

[11] An overview. Non-traditional Manufacturing processes.

[12] M. Kolb; Verlag moderne industrie: Waterjet Cutting, 2006.

[13] Shishkin, D. V.; Development of Ice Jet-Based Surface Processing Technology, NJIT, May 2002, c2002, PhD thesis.

[14] Patric Truchot, Pascal Mellinger and Robert Duchamp; Development of a Cryogenic water jet technique for biometal processing applications.

[15] K. Kluz, E.S. Geskin, D.V. Shishkin, B. Goldenberg, O.P. Petrenko; Formation and application of fine ice abrasive

[16] Grega Retelj; Merjenje razpršenosti visokohitrostnega vodnega curka. 2012.

[17] H. Orbanic, M. Junkar, I. Bajsic and A. Lebar; An instrument for measuring abrasive water jet diameter.2009

[18]]LDV– Laser Doppler Velocimetry [05-05-2013] Acces to: www.lavision.de/en/techniques/ldv_pdi.php

[19] PIV – Particle Image Velocimetry [05-05-2013] Acces to: www.dantecdynamics.com/Default.aspx?ID=820

[20] Heema Unadkat, Chris D. Rielly and Z. K. Nagy; PIV study of the flow field generated by a sawtooth impeller. 2011.

[21]] PIV Measurements [05-05-2013] Acces to: http://www.lasercenter.pl/piv.htm

[22] J. Estevadeordal, L. Goss: Piv with LED: Particle Shadow Velocimetry (PSV), 2005

[23] The high-speed camera [05-05-2013] Acces to: www.olympus-ims.com/en/hsv-products/i-speed-lt/

[24] Photography Sigma SD-14 [05-05-2013] Acces to: www.hometheaterhifi.com/volume_14_2/sigma-sd14-dslr-6-2007-part-1.html

[25] Laser induced fluorescence, dostopno na: http://en.wikipedia.org/wiki/Laser-induced_fluorescence

[26] Datasheet of Canon EOS 30D Digital from Japan CT 1-1008-000 [06-06-2013] Acces to: http://www.usa.canon.com/cusa/support/consumer/eos_slr_camera_systems/eos_digital_slr_cameras/eos_30d

[27] M. Jerman, A. Lebar and M. Junkar; Measurement and modelling of the water jet shape.

[28] Website[05-05-2013] Acces to : http://www.marcelapineros.com/_portfolio/surface/html/diagramas/en_variacion_de_ts_con_temperatura.htm

[29] Datasheet of LM3404/04HV 1.0A Constant Current Buck Regulatior for Driving High Power LEDs.[October 2006-Revised February 2010]

10 Attachment

10.1 Matlab code for analysis of the picture

Reference to this attachment was made from charter 5.4.

```
function kalibfak = kalibracija;
kalibfak = 5/320;
if kalibfak == 0
   sl = imread('d:\troika\JetShape\best one\IMG_1939.JPG');
   sl = rgb2gray(sl);
   sl = imadjust(sl'); sl = fliplr(sl);
   figure(1);
   imagesc(sl); colormap gray; axis equal; axis tight;
   tit_h=title('get 5 mm grooves in rectangle');
   rhkh = imrect(gca,[1240 1 100 3503]); %[xmin ymin width height]
   apik = iptgetapi(rhkh);
   set(tit_h,'String','press SPaCe to Continue'); pause
   rhk=round(apik.getPosition());
   %% napre
   %Y = sl(rhk(3):rhk(3)+rhk(4),round((rhk(1)+rhk(1)+rhk(2))/2)); Y=max(Y)-Y;
   % Y = double(sl(rhk(2):rhk(2)+rhk(4),round((rhk(1)+rhk(3)/2))));
   % %Y = double(max(Y)-Y); Y = smooth(Y,3);
   % Y = max(Y)-Y;
   % Y = smooth(Y,3);
   % X = linspace(1,length(Y),length(Y));
   % [P,S]=findpeaks(Y,'minpeakdistance',300,'npeaks',11,'threshold',30);
   % %[P,S]=findpeaks(Y,'npeaks',11);
   % enota_pxl = mean(diff(X(S)));
   % sipanje = std(diff(X(S))); f=10/enota_pxl;
   % figure(2); plot(X,Y); hold on; plot(X(S),P,'ro'); hold off;
   % figure(1); hold on; plot(round(rhk(1)+rhk(3)/2)*ones(size(S)), S+rhk(2),'r*')
   %% nap nap
   Y = sl(rhk(2):rhk(2)+rhk(4),rhk(1):rhk(1)+rhk(3));
   Y = imadjust(Y);
```

```
    dum = double(Y');
    ys = sum(dum);
    maska = find(yc>(mean(ys)+std(ys)));
    yc = ys; yc(maska) = (mean(ys)+std(ys)) * ones(size(maska));
    y = max(yc)-yc;
    dy = diff(y);
    maska = find(dy<0);
    dy(maska) = zeros(size(maska));
    %y(maska) = ones(size(maska));
    figure(2);plot(dy)
    %% nn
    %Y = double(max(Y)-Y); Y = smooth(Y,3);
    %Y = max(Y)-Y;
    %Y = smooth(Y,3);
    X = 1: length(dy); %linspace(1,length(dy),length(dy));
    [P,S]=findpeaks(dy,'minpeakdistance',300,'npeaks',11);
    %[P,S]=findpeaks(Y,'npeaks',11);
    enota_pxl = median(diff(X(S)))
    sipanje = std(diff(X(S))); f=10/enota_pxl;
    figure(2); plot(X,dy); hold on; plot(X(S),dy(S),'ro'); hold off;
    figure(1); hold on; plot(round(rhk(1)+rhk(3)/2)*ones(size(S)), S+rhk(2),'r*')

    kalibfak = 5/median(diff(X(S)));
end
```

10.2 Matlab code for referent of the picture

Reference to this attachment was made from charter 5.4.

```
kalibfak = kalibracija;
kalibfak = 5/320;
if kalibfak == 0
    sl = imread('D:\Jesus\photos\Referent_photo');
    sl = rgb2gray(sl);
```

```
sl = imadjust(sl'); sl = fliplr(sl);
figure(1);
imagesc(sl); colormap gray; axis equal; axis tight;
tit_h=title('get 5 mm grooves in rectangle');
rhkh = imrect(gca,[1240 1 100 3503]); %[xmin ymin width height]
apik = iptgetapi(rhkh);
set(tit_h,'String','press SPaCe to Continue'); pause
rhk=round(apik.getPosition());
%% napre
%Y = sl(rhk(3):rhk(3)+rhk(4),round((rhk(1)+rhk(1)+rhk(2))/2)); Y=max(Y)-Y;
% Y = double(sl(rhk(2):rhk(2)+rhk(4),round((rhk(1)+rhk(3)/2))));
% %Y = double(max(Y)-Y); Y = smooth(Y,3);
% Y = max(Y)-Y;
% Y = smooth(Y,3);
% X = linspace(1,length(Y),length(Y));
% [P,S]=findpeaks(Y,'minpeakdistance',300,'npeaks',11,'threshold',30);
% %[P,S]=findpeaks(Y,'npeaks',11);
% enota_pxl = mean(diff(X(S)));
% sipanje = std(diff(X(S))); f=10/enota_pxl;
% figure(2); plot(X,Y); hold on; plot(X(S),P,'ro'); hold off;
% figure(1); hold on; plot(round(rhk(1)+rhk(3)/2)*ones(size(S)), S+rhk(2),'r*')
%% nap nap
Y = sl(rhk(2):rhk(2)+rhk(4),rhk(1):rhk(1)+rhk(3));
Y = imadjust(Y);
dum = double(Y');
ys = sum(dum);
maska = find(yc>(mean(ys)+std(ys)));
yc = ys; yc(maska) = (mean(ys)+std(ys)) * ones(size(maska));
y = max(yc)-yc;
dy = diff(y);
maska = find(dy<0);
dy(maska) = zeros(size(maska));
%y(maska) = ones(size(maska));
figure(2);plot(dy)
```

```
    %% nn
    %Y = double(max(Y)-Y); Y = smooth(Y,3);
    %Y = max(Y)-Y;
    %Y = smooth(Y,3);
    X = 1: length(dy); %linspace(1,length(dy),length(dy));
    [P,S]=findpeaks(dy,'minpeakdistance',300,'npeaks',11);
    %[P,S]=findpeaks(Y,'npeaks',11);
    enota_pxl = median(diff(X(S)))
    sipanje = std(diff(X(S))); f=10/enota_pxl;
    figure(2); plot(X,dy); hold on; plot(X(S),dy(S),'ro'); hold off;
    figure(1); hold on; plot(round(rhk(1)+rhk(3)/2)*ones(size(S)), S+rhk(2),'r*')

    kalibfak = 5/median(diff(X(S)));
end
```

10.3 Arduino program to control of the camera

Reference to this attachment was made from charter 7.1.

```
// How to control the camera to make 30 photos with just push the Arduino bottom

int camT = 12;              //Give camera Trigger name
int camF = 11;              //give the camera Focus name
                      // the setup routine runs once when you press reset:
void setup() {            //Initialize the both digital pin as an output
  pinMode(camT, OUTPUT);
  pinMode(camF, OUTPUT);
}

void loop() {             //the loop routine runs over and over again forever
  digitalWrite(camF, HIGH);   //turn the camF on (HIGH is the voltage level)
  delay(200);             //Wait for a 20ms
  digitalWrite(camF, LOW);    //turn the camF off by making the voltage LOW
  delay(500);             //It's make for wake up the camera
  for (int i = 0; i<30; i++){ //To count from 0 to 30
```

```
  digitalWrite(camT, HIGH);
  delay(10);              //the time with the trigger on for each photo
  digitalWrite(camT, LOW) ;
  delay(750);              //the time with the trigger off between photos
 }
 while(1){                //To make a infinite bucle to put the arduino in
  delay(1000);             // state of wait until next order
 }
}
```

10.4 Table of Calibration factor for both shutter speed.

Reference to this attachment was made from charter 7.1.1

		Shutter speed 1250 s^{-1}		Shutter speed 2500 s^{-1}	
Shutter speed 1250 s^{-1}	**stand off**	**Force measurements**	**f=std/dM**	**Force measurements**	**f=std/dM**
Experiment1	**1**	0.53319	0.0188	0.53319	0.02875
	2	0.77824	0.03664	0.77824	0.0543
	3	0.77824	0.10174	0.77824	0.12571
	4	1.2574	0.10791	1.2574	0.12542
	5	1.2979	0.13219	1.2979	0.14201
Experiment2	**1**	0.79514	0.04187	0.79514	0.04372
	2	0.57291	0.11127	0.57291	0.10699
	3	0.95907	0.10321	0.95907	0.09759
	4	1.3072	0.08642	1.3072	0.08643
	5	1.3757	0.07717	1.3757	0.06406
Experiment3	**1**	0.50784	0.07716	0.50784	0.07646
	2	0.84838	0.06367	0.84838	0.05753
	3	0.88218	0.09098	0.88218	0.09063
	4	1.3875	0.08973	1.3875	0.06625
	5	1.63	0.11709	1.63	0.07341
Experiment4	**1**	0.62614	0.01524	0.62614	0.1664
	2	0.57375	0.02165	0.57375	0.17693
	3	0.78669	0.05689	0.78669	0.18571
	4	1.0943	0.06451	1.0943	0.17169
	5	1.2168	0.06886	1.2168	0.11628
Experiment5	**1**	0.54418	0.02887	0.54418	0.03883
	2	0.69121	0.0705	0.69121	0.07873
	3	1.1036	0.076	1.1036	0.08442
	4	1.0639	0.10045	1.0639	0.11136
	5	1.6934	0.14297	1.6934	0.11479
Experiment6	**1**	1.1585	0.00566	1.1585	0.00736
	2	1.2236	0.01422	1.2236	0.01971
	3	0.98696	0.03321	0.98696	0.04989
	4	2.2054	0.02122	2.2054	0.03069
	5	1.423	0.05481	1.423	0.05681
Experiment7	**1**	0.62361	0.03458	0.62361	0.01534
	2	0.42672	0.05507	0.42672	0.04875
	3	0.59319	0.09405	0.59319	0.09782
	4	0.57544	0.05031	0.57544	0.16401
	5	0.61347	0.08552	0.61347	0.196
Experiment8	**1**	0.43517	0.04953	0.43517	0.02982
	2	0.5915	0.06503	0.5915	0.03453

	3	0.79768	0.0733	0.79768	0.03896
	4	0.84246	0.10962	0.84246	0.06355
	5	0.71402	0.19201	0.71402	0.09679
Experiment9	**1**	0.33715	0.05407	0.33715	0.05328
	2	0.81965	0.04745	0.81965	0.03393
	3	0.63121	0.07934	0.63121	0.06994
	4	0.46137	0.19154	0.46137	0.16846
	5	1.1729	0.13455	1.1729	0.07053
Experiment10	**1**	0.68529	0.00738	0.68529	0.04019
	2	0.22899	0.03132	0.22899	0.07806
	3	0.90584	0.04353	0.90584	0.03017
	4	0.94217	0.09568	0.94217	0.08247
	5	0.76303	0.14002	0.76303	0.19585
Experiment11	**1**	1.4475	0.05	1.4475	0.00644
	2	0.7774	0.16355	0.7774	0.01912
	3	0.91767	0.18861	0.91767	0.04635
	4	0.94555	0.29156	0.94555	0.08287
	5	1.2329	0.18996	1.2329	0.08639
Experiment12	**1**	0.82218	0.00685	0.82218	0.01258
	2	1.5024	0.01193	1.5024	0.01922
	3	1.1078	0.05138	1.1078	0.06307
	4	1.1382	0.09156	1.1382	0.10132
	5	1.494	0.0922	1.494	0.10477
Experiment13	**1**	0.55178	0.08113	0.55178	0.03491
	2	0.30335	0.16263	0.30335	0.11967
	3	0.6591	0.0795	0.6591	0.08305
	4	0.60164	0.11784	0.60164	0.11478
	5	0.7681	0.13742	0.7681	0.10527
Experiment14	**1**	1.0486	0.03629	1.0486	0.02382
	2	0.84077	0.07595	0.84077	0.03651
	3	1.0089	0.08934	1.0089	0.07024
	4	0.67938	0.1438	0.67938	0.15871
	5	0.80866	0.12884	0.80866	0.123
Experiment15	**1**	0.50193	0.07094	0.50193	0.08133
	2	0.61094	0.07496	0.61094	0.11924
	3	0.96752	0.08207	0.96752	0.07699
	4	0.92189	0.1226	0.92189	0.10936
	5	0.93795	0.14253	0.93795	0.13191
Experiment16	**1**	0.5915	0.15094	0.5915	0.12185
	2	0.7343	0.20512	0.7343	0.16144
	3	0.48249	0.36721	0.48249	0.3223
	4	0.68529	0.24711	0.68529	0.23828
	5	0.96668	0.14645	0.96668	0.14352

Experiment17	**1**	0.57629	0.11922	0.57629	0.11941
	2	0.68445	0.17324	0.68445	0.16372
	3	1.2523	0.11821	1.2523	0.10469
	4	0.96414	0.16796	0.96414	0.15023
	5	0.80359	0.19986	0.80359	0.15703
Experiment18	**1**	0.54502	0.11297	0.54502	0.12354
	2	0.91091	0.1129	0.91091	0.1171
	3	1.4213	0.1048	1.4213	0.0987
	4	1.2616	0.1412	1.2616	0.12584
	5	1.2878	0.14092	1.2878	0.11978

STATEMENT

The undersigned *Jesús Gil Cano*, born on 06/ July/ 1987 have done the master thesis by myself under the guidance of Mentor dr. Mihael Junkar and Co-Mentor dr. Andrej Lebar.

The project manager was Lorenzo Ros McDonnell.

Jesús Gil Cano:

…….